Article

Weak Interactions in Cocrystals of Isoniazid with Glycolic and Mandelic Acids

Raquel Álvarez-Vidaurre [1], **Alfonso Castiñeiras** [1,*], **Antonio Frontera** [2], **Isabel García-Santos** [1], **Diego M. Gil** [3], **Josefa M. González-Pérez** [4], **Juan Niclós-Gutiérrez** [4] and **Rocío Torres-Iglesias** [1]

1   Department of Inorganic Chemistry, Faculty of Pharmacy, University of Santiago de Compostela, 15782 Santiago de Compostela, Spain; raquel.alvarez.vidaurre@rai.usc.es (R.Á.-V.); isabel.garcia@usc.es (I.G.-S.); rocio.torres.iglesias@rai.usc.es (R.T.-I.)
2   Department of Química, Universitat de les Illes Balears, Crta. de Valldemossa km 7.5, 07122 Palma de Mallorca, Spain; toni.frontera@uib.es
3   INBIOFAL (CONICET – UNT), Instituto de Química Orgánica, Facultad de Bioquímica, Química y Farmacia, Universidad Nacional de Tucumán, Ayacucho 471, T4000INI San Miguel de Tucumán, Argentina; dmgil@fbqf.unt.edu.ar
4   Department of Inorganic Chemistry, Faculty of Pharmacy, University of Granada, 18071 Granada, Spain; jmgp@ugr.es (J.M.G.-P.); jniclos@ugr.es (J.N.-G.)
*   Correspondence: alfonso.castineiras@usc.es

Abstract: This work deals with the preparation of pyridine-3-carbohydrazide (isoniazid, inh) cocrystals with two α-hydroxycarboxylic acids. The interaction of glycolic acid (H_2ga) or d,l-mandelic acid (H_2ma) resulted in the formation of cocrystals or salts of composition $(inh)\cdot(H_2ga)$ (**1**) and $[Hinh]^+[Hma]^-\cdot(H_2ma)$ (**2**) when reacted with isoniazid. An N'-(propan-2-ylidene)isonicotinic hydrazide hemihydrate, $(pinh)\cdot1/2(H_2O)$ (**3**), was also prepared by condensation of isoniazid with acetone in the presence of glycolic acid. These prepared compounds were well characterized by elemental analysis, and spectroscopic methods, and their three-dimensional molecular structure was determined by single crystal X-ray crystallography. Hydrogen bonds involving the carboxylic acid occur consistently with the pyridine ring N atom of the isoniazid and its derivatives. The remaining hydrogen-bonding sites on the isoniazid backbone vary based on the steric influences of the derivative group. These are contrasted in each of the molecular systems. Finally, Hirshfeld surface analysis and Density-functional theory (DFT) calculations (including NCIplot and QTAIM analyses) have been performed to further characterize and rationalize the non-covalent interactions.

Keywords: isoniazid; cocrystals; glycolic acid; DL-mandelic acid; X-ray structure; Hirshfeld surface analysis; DFT calculations

1. Introduction

As an important part of supramolecular chemistry, crystal engineering has been the subject of continuous research in solid and materials science for many years, and cocrystals have been a research area for more than 150 years, used in many industries, such as pharmaceuticals, textiles, paper, chemical, photographic processing, propelling and electronics, among others [1]. Rapid development in this field has revealed the use of a variety of organic components with specific functional groups to create supramolecular arrays through the coordination of metals or non-covalent forces, presenting interesting structures and useful properties. In this context, numerous recent examples of multicomponent crystals are known, the assembly of which is driven by non-covalent interactions, mainly hydrogen bonding with or without charge assistance [2]. Acid-base binary cocrystals is an important technological topic in pharmaceutical science that has attracted scientific and pharmaceutical interest in recent decades due to their potential ability to modify important properties of active pharmaceutical ingredients (APIs) such as solubility, dissolution rate, bioavailability, hygroscopicity, and/or thermal stability [3]. Furthermore, the formation of

these multicomponent crystals does not lead to changes in the nature of the API, unlike the situation observed during salt formation, where the API must or may be protonated [4]. Co-crystals containing heterocyclic nitrogen bases have been studied extensively, especially those with mono- and di-carboxylic acids as co-formers, and it can be concluded that the interaction between a carboxylic acid and a pyridine is a supramolecular synthon of frequent use in crystal engineering that may exist as a cocrystal ($CO_2H \cdots N$) or as salt ($CO_2^- \cdots HN^+$) [5–9]. However, few studies are known of cocrystals with carboxylic acids as co-formers that also contain a hydroxyl moiety [10], such as the α-hydroxycarboxylic acids, particularly against isonicotinic acid hydrazide (isoniazid, inh) (Scheme 1) as API.
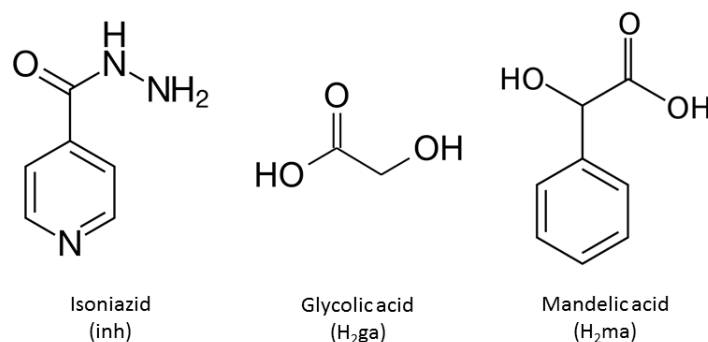
Scheme 1. Molecular structures of the formers/coformers.

In this field of research, from a crystal engineering viewpoint, isoniazid represents an interesting compound for cocrystal design, and is an important API that, among other uses, is applied in combination with rifampicin, pyrazinamide and ethambutol for the treatment of tuberculosis, which are known as fixed-dose combinations [11]. Furthermore, the reaction of inh with ketones is used to modify or improve their molecular efficacy at the biological level [12]. For example, in the compound obtained with 2-propanone, an increase in activity against Mycobacterium tuberculosis is observed with respect to inh [13]. The chemical structure of inh possesses pyridine and carbohydrazide functional groups capable of forming hydrogen bonds, leading to the formation of supramolecular homo-synthons (hydrazide–hydrazide) and hetero-synthons (pyridine–carboxylic acid, hydroxyl–pyridine, amide–amide, hydroxyl–amide) [14,15]. Therefore, isoniazid can be considered a suitable candidate or appropriate molecule for studies in the field of pharmaceutical cocrystals.

As possible co-formers of salts or cocrystals against inh, we have considered α-hydroxycarboxylic acids, glycolic (H_2ga) and D,L-mandelic (H_2ma) [16,17] (Scheme 1). The common molecular features of these analogous co-formers are expected to influence the molecular packing in crystals with both directional H-bonds and no directional van der Waals interactions. From the point of view of hydrogen bonding, each of them contains three H-acceptor oxygen atoms and two donor O–H groups. With respect to other mono-carboxylic acids, α-hydroxycarboxylic acids contain a hydroxyl group in adjacent carbon, and therefore have an additional set of sites capable of hydrogen bonding, both of a donor and an acceptor character. Furthermore, in relation to dicarboxylic acids, proton transfer of the hydroxyl group is lower than that of the carboxylic group, thereby favoring cocrystals formation. On the other hand, the presence of a phenyl group in H_2ma with respect to H_2ga allows to estimate the influence of the ring in crystalline packing and, if applicable, the existence of other interactions such as ring–ring stacking. Both participate in many biochemical processes and have widespread applications both in biological systems and in industry. Thus, glycolic acid, a common component of sugarcane juice and other foods, has an important role in photosynthesis and plant respiration and is a known precursor to oxalate in humans [18], while mandelic acid is a useful precursor to various drugs, for example, homatropine and cyclandelate, which are esters of mandelic acid, and is also known to have antibacterial properties [19] and has been studied in the preparation of antitumor compounds [20]. Taking into account the previous considerations, the main aim

of this work has been the design, preparation and characterization of the physicochemical properties, and identification of recurrent supramolecular patterns within a new set of multicomponent pharmaceutical crystals that involve isoniazid with glycolic and DL-mandelic acids as co-formers (Scheme 1). The non-covalent interactions observed in their solid state have been further analyzed and characterized using Hirshfeld surface analysis and density functional dispersion (DFT) calculations.

2. Experimental and Theoretical Methods

2.1. Materials and Methods

Glycolic acid, mandelic acid and isoniazid were purchased from Sigma-Aldrich (Sigma-Aldrich. Inc., Tres Cantos, Madrid, Spain). Commercially available solvents were used as received without further purification.

Microanalyses (C, H and N) were carried out in a Carlo-Erba 1108 elemental analyzer (CARLO ERBA Reagents SAS, Chaussée du Vexin, France). FT-IR spectra (Supplementary Materials) were recorded from KBr pellets over the range 4000–400 cm^{-1} on a Bruker IFS-66v spectrometer (Bruker Corporation, Billerica, MA, USA). ^1H NMR spectra (Supplementary Materials) in DMSO-d_6 were run on Bruker AMX 300 instrument, using tetramethylsilane (TMS) as internal reference.

2.2. Crystallography

Colorless crystals of (inh).(H_2ga) (**1**), [Hinh]$^+$[Hma]$^-$·(H_2ma) (**2**) and (pinh)·1/2(H_2O) (**3**) were successively mounted on a glass fiber and used for data collection. Crystal data were collected at 100(2) K, using a Bruker X8 KappaAPEXII diffractometer (Bruker AXS Inc., Madison, Wisconsin, USA). Graphite mono-chromated MoKα radiation (λ = 0.71073 Å) was used throughout. The data were processed with APEX3. [21] and corrected for absorption using SADABS [22]. The structure was solved by direct methods using the program SHELXS-2013 [23] and refined by full-matrix least-squares techniques against F^2 using SHELXL-2013 [23]. Positional and anisotropic atomic displacement parameters were refined for all non-hydrogen atoms. Hydrogen atoms were located in difference maps and refined isotropically, but those bonded to carbon atoms were included as fixed contributions riding on attached atoms with isotropic thermal parameters 1.2/1.5 times those of their carrier atoms. For **3**, the Flack parameter (absolute structure parameter) was calculated to be 0.20(9) for the present structure and 0.80(9) for the inverted structure, thus providing strong evidence that the absolute structure has been assigned correctly [24]. Molecular graphics were generated with DIAMOND (Crystal Impact GbR, Bonn, Germany) [25]. Crystal data, experimental details and refinement results are summarized in Table 1. The structures were deposited at the Cambridge Crystallographic Data Centre with CCDC Nos. 2041154-2041156, for **1** to **3**, respectively.

2.3. Cocrystal Screening

For each system, mixtures of the α-hydroxycarboxylic acid and isoniazid in 1:1 molar ratios were prepared and thoroughly ground using an agate mortar and pestle for 5–7 min in order to obtain the physical mixture. After the addition of several drops of the appropriate solvent the clear, non-saturated solution was poured on a 5 mL vial and was allowed to evaporate at ambient conditions until crystals suitable for X-ray diffraction formed.

Table 1. Crystal data and structure refinement for the compounds (inh)·(H$_2$ga) (**1**), [Hinh]$^+$[Hma]$^-$·(H$_2$ma) (**2**) and (pinh)·1/2(H$_2$O) (**3**).

Compound	1	2	3
Empirical formula	C$_8$H$_{11}$N$_3$O$_4$	C$_{22}$H$_{23}$N$_3$O$_7$	C$_9$H$_{12}$N$_3$O$_{1.5}$
Formula weight	213.20	441.43	186.22
Crystal system	Monoclinic	Monoclinic	Orthorhombic
Space group	$P2_1/n$	$P2_1/c$	*Aba*2
Unit cell dimensions			
a/Å	3.8930(3)	5.6049(5)	18.8351(5)
b/Å	9.9754(5)	24.388(3)	12.6568(4)
c/Å	23.6410(12)	15.1471(16)	8.0435(3)
α/°	90	90	90
β/°	92.480(3)	92.025(7)	90
γ/°	90	90	90
Volume/Å^{-3}	917.22(10)	2069.2(4)	1917.51(11)
Z	4	4	8
Calc. density/Mg/m^3	1.544	1.417	1.290
Absorp. coefc./mm^{-1}	0.125	0.107	0.091
F(000)	448	928	792
Crystal size	0.19 × 0.14 × 0.05	0.46 × 0.40 × 0.03	0.66 × 0.24 × 0.13
θ range/°	1.724–26.399	2.145–28.280	2.163–36.313
Limiting indices/*h,k,l*	−4/4, −12/12, −29/29	−7/7, −32/32, −20/19	−30/31, −20/21, −13/13
Refl. collect/unique (R_{int})	13443 / 1879 [0.0501]	32295 / 5150 [0.0703]	76482 / 4651 [0.0447]
Completeness θ/°	25.242–99.9	25.242–99.9	25.242–99.9
Absorp. correct.	Multi-scans	Multi-scans	Multi-scans
Max./min. transm.	1.0000/0.8327	1.000/0.868	1.000/0.883
Data/parameters	1879/156	5150/317	4651/132
Goodness-of-fit on F^2	1.047	1.003	1.030
Final R indices	R_1 = 0.0417, wR_2 = 0.0901	R_1 = 0.0501, wR_2 = 0.0985	R_1 = 0.0341, wR_2 = 0.0899
R indices (all data)	R_1 = 0.0645, wR_2 = 0.0980	R_1 = 0.0888, wR_2 = 0.1114	R_1 = 0.0402, wR_2 = 0.0938
Largest dif. peak/hole	0.224/−0.280	0.300/−0.266	0.373 /−0.179

2.4. Cocrystal Synthesis

(inh)·(H$_2$ga) (**1**). Glycolic acid (0.150 g, 1.97 mmol) and isoniazid (0.270 g, 1.97 mmol). Ethyl acetate or cyclohexane (10 mL). Colorless crystals after fifty days. Melting Point. (MP) (°C): 120–125. Elemental analysis: Found: C, 45.2; H, 5.36; N, 19.6. Calculated (%) for C$_8$H$_{11}$N$_3$O$_4$: C, 45.1; H, 5.20; N, 19.7. IR (ν_{max}/cm^{-1}): 3408m, 3232m, 3172m, 3051m, 3029m, 2923m, 2846m, 1672s, 1638m, 1602m, 1576m, 1553m, 1534m, 1497m, 1469m, 1431m, 1417m, 1384w, 1323m, 1294m, 1267m, 1223w, 1179m, 1096s, 996w, 897w, 850m, 798w, 760w, 679m, 622w. ^{1}H NMR (Dimethyl sulfoxide, DMSO-d$_6$, δ/ppm): 3.91 (CH$_2$, NH$_2$), 7.71–7.73 (py), 8.69–8.70 (py).

[Hinh]$^+$[Hma]$^-$·(H$_2$ma) (**2**). Mandelic acid (0.152 g, 0.9 mmol) and isoniazid (0.137 g, 0.9 mmol). Water (4.5 mL). Colorless crystals after two days. MP (°C): 115–120. Elemental analysis: Found: C, 60.1; H, 4.92; N, 9.5. Calculated (%) for C$_{22}$H$_{23}$N$_3$O$_7$: C, 59.9; H, 5.25; N, 9.5. IR (ν_{max}/cm^{-1}): 3413s, 3194m,br, 3031m, 2926m, 1694s, 1613m, 1600m, 1560m, 1494m, 1454m, 1414s, 1335m, 1266s, 1222s, 1213m, 1186s, 1081mm, 1061s, 1014m, 933w, 874w, 851m, 754m, 733s, 692s, 680m, 608w. ^{1}H NMR (DMSO-d$_6$, δ/ppm): 5.02 (OH, alcohol), 5.69 (CH), 7.28–7.43 (ph), 8.69 (1H, N1H), 7.71–7.71 (py), 8.69–8.71 (py), 10.02 (OH, carboxylic).

(pinh)·1/2(H$_2$O) (**3**). Glycolic acid (0.150 g, 1.97 mmol) and Isoni-acid (0.270 g, 1.97 mmol). Acetone (0.5 mL). Colorless crystals after six days. MP (°C): 155–160. Elemental analysis: Found: C, 58.3; H, 6.24; N, 22.2. Calculated (%) for C$_9$H$_{12}$N$_3$O$_{1.5}$: C, 58.0; H, 6.49; N, 22.6. IR (ν_{max}/cm^{-1}): 3423m,br, 3303m, 3189s, 3080m, 3031s, 2917m, 2824m, 2692w, 1655s, 1635s, 1599m, 1551s, 1535s, 1491m, 1434m, 1407m, 1374m, 1322w, 1298s, 1266w, 1220w,

1208m, 1149m, 1093w, 1062w, 1029m, 990w, 904w, 836m, 758m, 727w, 671s, 623m. ^{1}H NMR (DMSO-d$_6$, δ/ppm): 1.94 (CH$_3$), 2.02 (CH3), 7.71–7.73 (py), 8.71–8.72 (py), 10.70 (NH).

The co-crystal preparation for each system was repeated in other solvents of different polarity, such as dichloromethane, formamide, N,N-Dimethylformamide (DMF), chloroform, acetonitrile, isopropyl alcohol, ethanol, methanol, CCl$_4$, THF and toluene, with little or no yield.

2.5. Hirshfeld Surface Analysis

The Hirshfeld surface analysis [26] and associated two-dimensional fingerprint plots [27,28] were performed using the *CrystalExplorer17.5* (University of Western Australia, Perth, Australia) program [29].

The crystallographic information file (.cif) of each compound was imported into CrystalExplorer and High resolution Hirshfeld surfaces were mapped by using the d_{norm}, shape index and curvedness functions. The normalized contact distance (d_{norm}) is a symmetric function based on both d_e (the distance from the point to the nearest nucleus external to the surface) and d_i (the distance to the nearest nucleus internal to the surface), relative to their respective van der Waals (vdW) radii. This function enables identification of different regions of particular importance to intermolecular interactions [27]. A color scale of red (shorter than vdW separation), white (equal to vdW separation), and blue (longer than vdW separation) is used to visualize the relevant intermolecular contacts in the d_{norm} surface. The 3D d$_{norm}$ surfaces were mapped over a fixed scale of −0.075 a.u. (red) to 0.50 a.u. (blue), shape index mapped in the color range of −1.00 au (concave) to 1.00 a.u. (convex), and curvedness in the color range of −4.00 a.u. (flat) to 0.40 a.u. (singular). A final analysis of the intermolecular interactions and their contribution to crystal packing was performed by analyzing the 2D fingerprint (FP) plots. These FP plots were displayed by using the expanded 0.6–2.8 Å range, including reciprocal contacts.

2.6. Theoretical Methods

The energies reported herein were computed either using Gaussian-16 [30] at the PBE0 [31] -D3 [32] /def2-TZVP [33] level of theory using the supramolecular approach or using the quantum theory of "atoms-in-molecules" [34] at the same level by means of the AIMAll program (TK Gristmill Software, Overland Park, KS, USA) [35]. For the former the BSSE correction [36] has been applied and for the latter we have used the kinetic energy density values at the bond critical points that emerge upon complexation, applying the methodology proposed by Espinosa et al. [37]. This methodology has been recently used to evaluate non-covalent interactions in the solid state [38–45]. The NCI plot iso-surfaces [46,47] have been generated using the AIMAll program [35] using the PBE0-D3/def2-TZVP wavefunction.

3. Results and Discussion

The three crystals were obtained from the crystallization of solutions prepared by reacting the isoniazid with glycolic or mandelic acids in a molar ratio 1:1. Although the X-ray diffraction data were taken at 100 K, solid handling was always done at room temperature.

The co-crystallization processes have been carried out considering the pK_a of isoniazid, and as co-formers the glycolic and D,L-mandelic acids. Isoniazid has three pK_a values: 1.8 based on hydrazine nitrogen, 3.6 based on pyridine nitrogen and 10.8 based on acidic group [48]. This makes the pyridine the more basic of the two, and in the presence of a carboxylic acid group it is protonated first. The pK_a of the glycolic acid molecule is 3.2 [49], giving a value of $\Delta pK_a = pK_{a(base)} - pK_{a(acid)} = 0.4$ for the combination of the acid with the pyridine group, and of −1.4 of the acid with the hydrazine nitrogen. Regarding mandelic acid, the pK_a is 3.4 and the values of ΔpK_a are 0.2 and −1.6, respectively. This range has been given by previous researchers as a rule of thumb where the result cannot be easily predicted. [50]. In general, a $\Delta pK_a > 3$ will be expected to form a salt, while a $\Delta pK_a < 0$ almost certainly results in a neutral co-crystal. It is the narrow region between 0 and 3 that

does not allow for accurate predictions [51]. The ΔpK_a for the acid and amine combination is $-1.4/-1.6$, which would predict that no proton transfer should occur since the value is less than 0. However, in the case of D,L-mandelic acid, crystallographic results confirm that proton transfer occurs. A caveat to the calculations is that the reported pK_a for the two molecules, isoniazid and glycolic acid or D,L-mandelic acid, depends on the solvent used and its polarity. While compound **1** has been obtained in ethyl acetate (ϵ = 6.2) or cyclohexane (ϵ = 2.02), compound **2** has been crystallized from water (ϵ = 80). Furthermore, it should be noted that a comprehensive study of 6465 crystalline compounds containing ionized (A$^+$B$^-$) and non-ionized (AB) acid-base pairs in the Cambridge Structural Database (CSD), at $1 < \Delta$p$K_a < 2$ values, shows that the occurrences of AB and A$^+$B$^-$ are practically the same [51].

3.1. Structural Description and Supramolecular Analysis

The geometric parameters of isoniazid, glycolic acid and D,L-mandelic acid within the structures of compounds **1** and **2** are comparable to those of free conformers and therefore are not discussed here in detail. The geometrical parameters of hydrogen bonding are shown in Table 2.

Table 2. Hydrogen bond parameters [Å, °] for (inh)·(H$_2$ga) (**1**), [Hinh]$^+$[Hma]$^-$·(H$_2$ma) (**2**) and (pinh)·1/2(H$_2$O) (**3**). Letters included as superscripts refer to symmetry codes shown in text and figures.

Cmpnd	D–H···A	D–H	H···A	D···A	∠DHA	Symmetry Code
1	N12–H12A···O12[a]	0.84(2)	2.43(2)	3.2617(19)	168.1(19)	x − 1, y + 1, z
	N12–H12A···O13[a]	0.84(2)	2.59(2)	3.1168(19)	121.5(17)	
	N11–H11A···O20[b]	0.89(2)	2.14(2)	3.022(2)	167.4(18)	−x + 1/2, y + 1/2, −z + 1/2
	N11–H11B···O13[a]	0.89(2)	2.62(2)	3.049(2)	110.2(16)	
	O11–H11···N17[c]	1.00(3)	1.60(3)	2.6064(19)	178(2)	−x + 2, −y + 1, −z
	O13–H13A···O20[d]	0.89(3)	1.91(3)	2.7399(18)	154(2)	−x+1/2, y−1/2, −z + 1/2
	O13–H13A···N11[d]	0.89(3)	2.60(3)	3.294(2)	135(2)	
	C15–H15···O12[e]	0.95	2.53	3.118(2)	119.8	x, y + 1, z
	C18–H18···O11[f]	0.95	2.49	3.235(2)	134.8	X − 1, y, z
2	O11–H11···N37[a]	1.01(2)	1.62(2)	2.6252(16)	171(2)	X + 1, −y + 1/2, z + 1/2
	O13–H13···O21[b]	0.87(2)	2.51(2)	3.0671(16)	122.1(17)	X − 1, y, z
	O13–H13···O23[b]	0.87(2)	1.86(2)	2.7106(15)	162(2)	
	O23–H23···O12	0.97(2)	1.91(2)	2.7716(18)	146.3(19)	
	O23–H23···O13	0.97(2)	2.42(2)	3.1756(16)	135.1(18)	
	N31–H31A···O22[c]	0.94(2)	1.87(2)	2.7971(17)	170.1(18)	x, −y + 1/2, z + 1/2
	N31–H31B···O13[d]	0.96(2)	1.85(2)	2.807(2)	172.7(19)	−x + 1, y− 1/2, −z + 1/2
	N31–H31C···O21[e]	1.07(2)	1.64(2)	2.677(2)	162.5(19)	x − 1, −y + 1/2, z + 1/2
	N32–H32···O22[e]	0.96(2)	1.75(2)	2.7009(18)	168.5(18)	
	C12–H12···O12[b]	0.98	2.57	3.4869(19)	155.7	
	C35–H35···O22[e]	0.93	2.55	3.411(2)	154.8	
3	N12–H12A···O20[a]	0.86(2)	2.02(2)	2.8683(13)	169.7(19)	−x + 1/2, y, z + 1/2
	O1–H1A···N17[b]	0.89(2)	2.00(2)	2.8714(12)	168(2)	−x + 1/2, y, z − 1/2
	C16–H16···N11[c]	0.95	2.58	3.4475(15)	152.1	x, y − 1/2, z + 1/2
	C19–H19···O1[d]	0.95	2.42	3.3328(11)	161.2	−x + 1/2, y + 1/2, z
	C21–H21B···O20[a]	0.98	2.57	3.0523(14)	110.1	−x + 1/2, y, z + 1/2
	C22–H22C···O1[e]	0.98	2.43	3.3599(15)	159.0	x, y + 1/2, z − 1/2

From the point of view of classical hydrogen bonds, isoniazid contains two donor atoms (N11, N12) and three acceptor atoms (N11, N17, O20), and the alpha-hydroxycarboxylic acids, glycolic and mandelic, also contain two donor atoms (O11, O13) and three acceptor atoms (O11, O12, O13). Therefore, in compounds **1** and **2**, numerous hydrogen bonding interactions are to be expected that will govern crystalline packing and, by extension, various physicochemical properties.

Compound **1**. In the isoniazid−glycolic acid cocrystal (**1**) the asymmetric unit contains one isoniazid molecule and one glycolic acid molecule (Figure 1a). Glycolic acid is hydrogen-bonded to isoniazid pyridine N through O−H···N. The angle between the carboxyl group plane and the pyridyl ring plane is 4.9°. A weak pyridyl−glycolic acid C−H···O hydrogen bond results in an $R_2^2(7)$ ring motif (Figure 1b). This synthon has also been observed in other isoniazid cocrystals with carboxylic acids [4]. From a crystal engineering viewpoint, inh is well known to form pyridine–carboxylic acid hetero-synthons with carboxylic acids. According to a recent study, 39 structures of inh cocrystals have been reported with co-formers containing COOH groups, representing approximately 40% of all inh structures deposited in the CSD, where the acid-pyridine synthon is the most recurrent and is present in approximately 87% of structures [4]. Furthermore, each isoniazid molecule is linked by hydrogen bonding to its two other nearest neighbor molecules through N-H···O, as donor and acceptor, respectively, forming zigzag chains parallel to the b-axis (Figure 2a) which in turn are linked through head-to-tail glycolic acid molecules by two new hydrogen bonds O−H···N and O−H···O, so a step sequence −H$_2$ga-inh-H$_2$ga-inh− is established along the c-axis (Figure 2b). In this way a double layer is formed (Figure 2c) that extends in parallel to the bc-plane (Figure 2d). In the crystal packing, several hydrogen bond motifs of graph-set $R_4^4(10)$ are observed between the nitrogen atom of the pyridine ring, N17, and the oxygen atom of the carboxylic group, O11, as acceptors and with this same atom and the carbon atom neighboring the pyridine nitrogen, C18, of closer symmetric center molecules, as donors (Figure 3). In the network, there are also three rings attached at an angle, of graph-set motifs $R_1^2(5)$, $R_2^1(7)$, $R_5^3(12)$ (Figure 3).
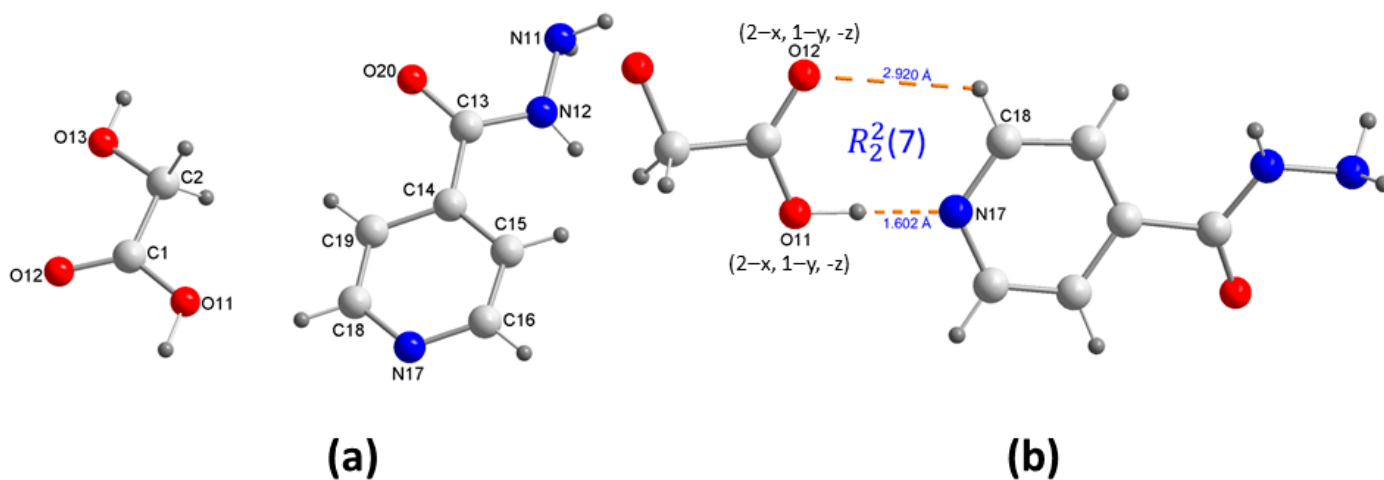

Figure 1. (**a**) Asymmetric unit of (inh)·(H$_2$ga) (**1**) showing the atom-numbering scheme, and (**b**) detail of carboxylic–pyridine hydrogen bonding interaction and $R_2^2(7)$ ring motif.
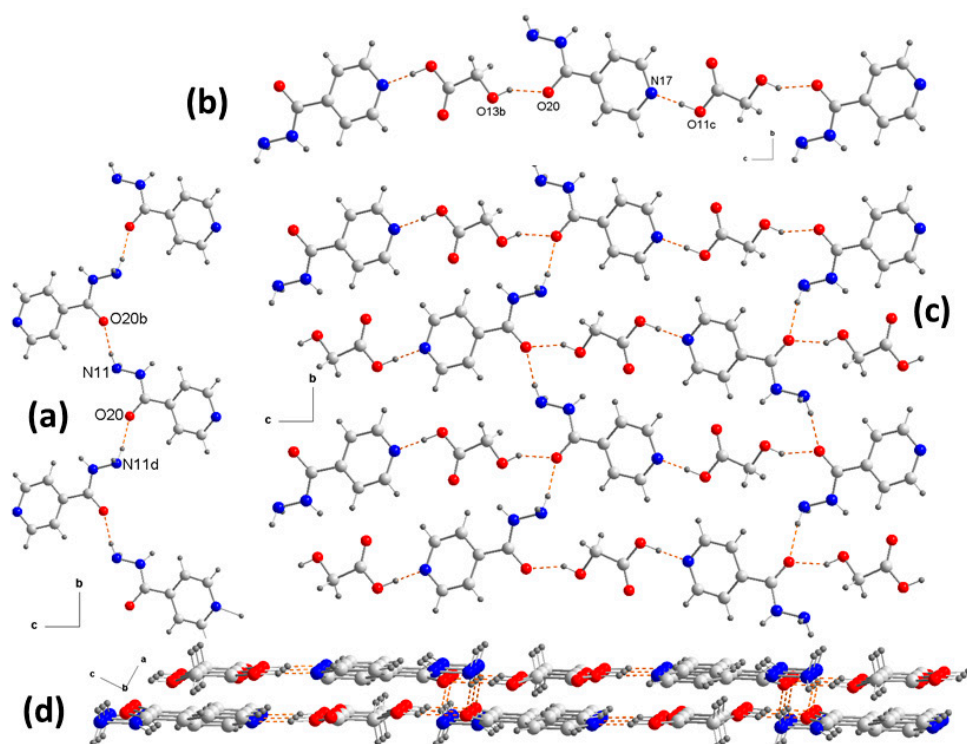
Figure 2. Perspective view of (**a**) zigzag chains, (**b**) chains ... inh-H$_2$ga ... ; (**c**) view of double layers; (**d**) detail of layer parallel to the plane "cb".
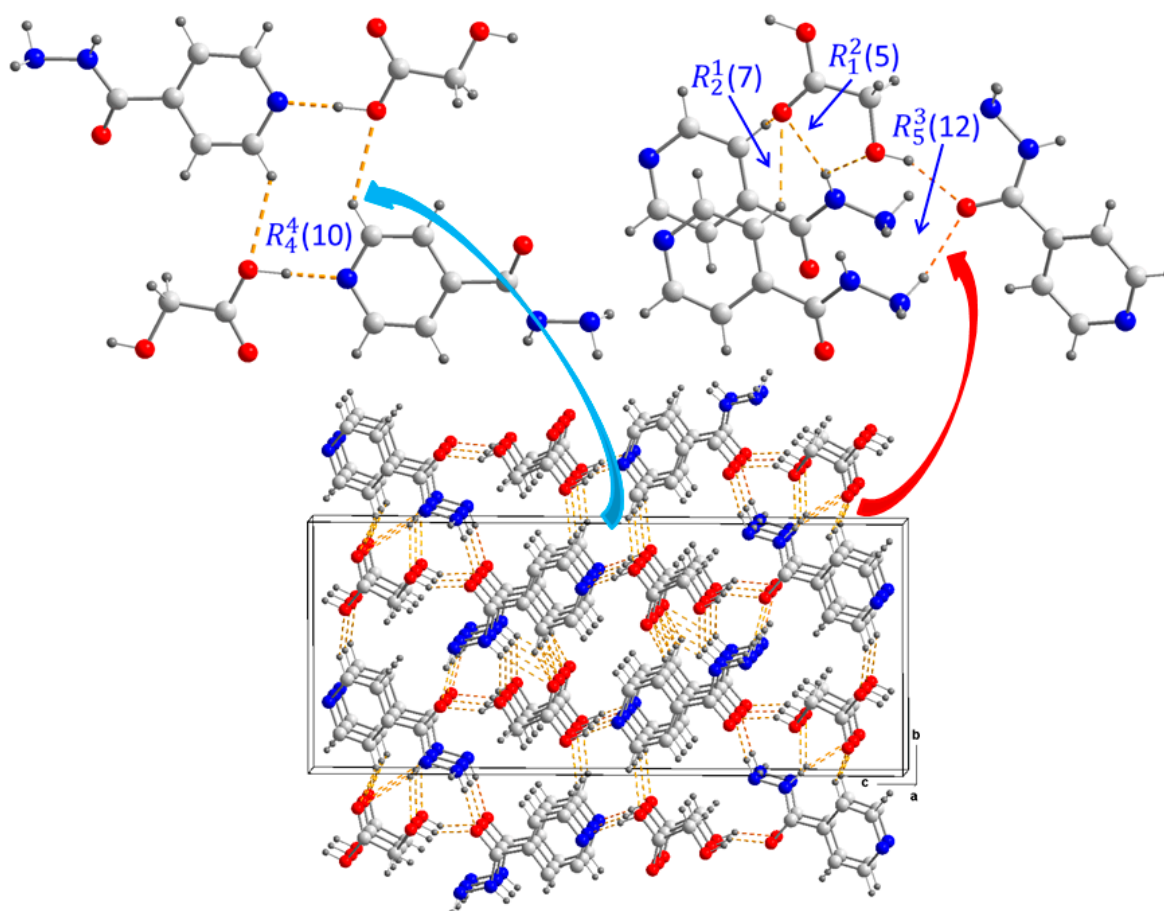

Figure 3. Crystal packing of **1** showing the different hetero-synthons.

Compound **2**. Using a 1:1 ratio of DL-mandelic racemic acid and achiral isoniazid, co-crystallization by mechanochemistry and liquid-assisted grinding in the presence of water results in the formation of a salt. The asymmetric unit of **2** contains one isoniazide-ammonium cation (Hinh)$^+$, one (D)-mandelate anion, and one (L)-mandelic acid molecule of crystallization. Figure 4a shows the molecular structure of **2**. In the unusual protonated isoniazid cation, the (D)-mandelate anion transfers its proton to the hydrazine nitrogen atom, N30, giving rise to a robust hydrogen bond N$^+$−H⋯O$^-$ that is supported by N−H⋯O$^-$ and C−H⋯O$^-$ hydrogen bonds, resulting in $R_2^2(7)$ and $R_2^1(7)$ rings, respectively (Figure 4b). The neutral (L)-mandelic acid molecule of crystallization is hydrogen bonded to the pyridine nitrogen atom, N35, of the isoniazid-ammonium cation through O−H⋯N. The angle between the plane of the carboxyl group and the plane of the pyridyl ring is 9.23°, somewhat higher than that observed in compound **1**. A weak hydrogen bond C−H⋯O, pyridyl-mandelic acid, results in a $R_2^2(7)$ ring motif (Figure 4b).

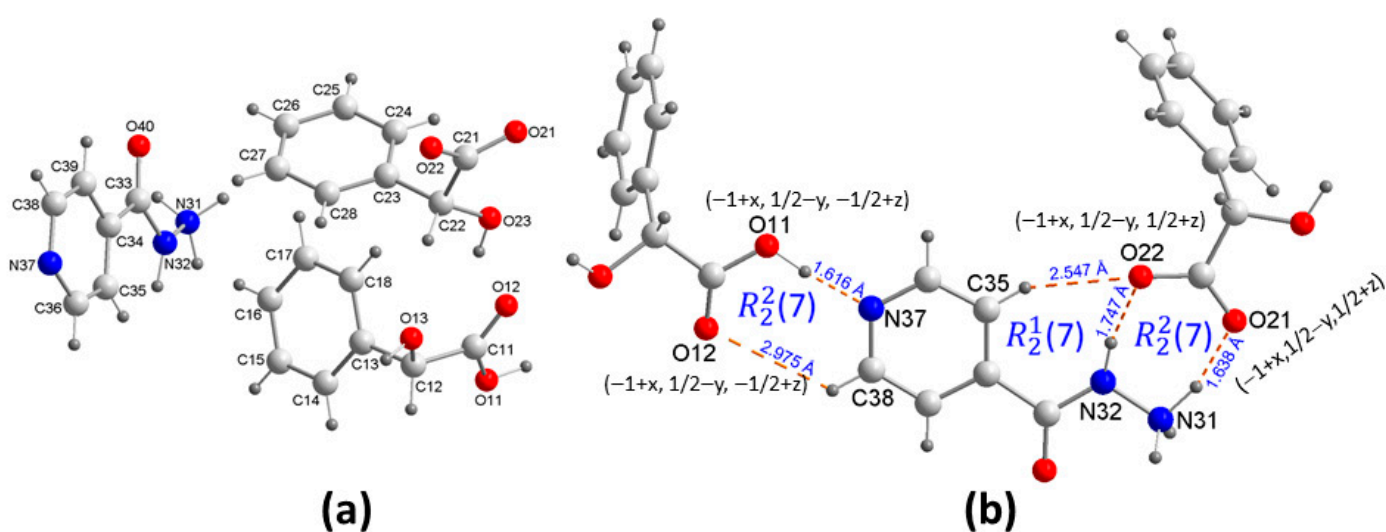**Figure 4.** (**a**) Asymmetric unit of [Hinh]$^+$[Hma]$^-$(H$_2$ma) (**2**) showing the atom-numbering scheme, and (**b**) detail of rings motif between the protonated.

In a more in-depth analysis of the interactions, it is observed that each [Hinh]$^+$ cation uses its four NHs to form strong hydrogen bonds N−H⋯O with an acid molecule and an anion [Hma]$^-$ and two more with a second anion forming the ring motif hetero-synthons $R_2^2(7)$ discussed above. Furthermore, the pyridine nitrogen atom is an acceptor of a fifth classical hydrogen bond with a second H$_2$ma molecule through the O−H bond of its carboxylic group, and uses the C25–H bond to form a non-classical hydrogen bond with the carbonyl oxygen atom, O22^e (−1 + x, 1/2−y, 1/2 + z), resulting in a hetero-synthon of graph-set $R_2^1(7)$ (Figure 5a). For its part, the mandelate and the mandelic acid molecule form two synthons of graph-set $R_1^2(5)$ acting as the donor of the hydroxyl OH of [Hma]$^-$ and as acceptors the carbonyl and hydroxyl oxygen atoms of the solvation molecule (Figure 5b).

This pair interacts in turn with two cations so that the acid molecule is bound to one cation and two anions while it interacts with the second isoniazid-ammonium (Figure 5b). Thus, layers parallel to "ac" plane are formed that contain the sequence ⋯ [Hinh]$^+$ ⋯ [Hma]$^-$ ⋯ H$_2$ma ⋯ along the axis "c" (Figure 6a). Two of these layers, inverted one with respect to the other, interact with each other through hydrogen bonds N−H⋯O, so that the phenyl rings point outwards (Figure 6b), giving rise to a stacking in the direction of the axis "b" that originates a 3D network where the double layers do not maintain any interaction with each other (Figure 6b).
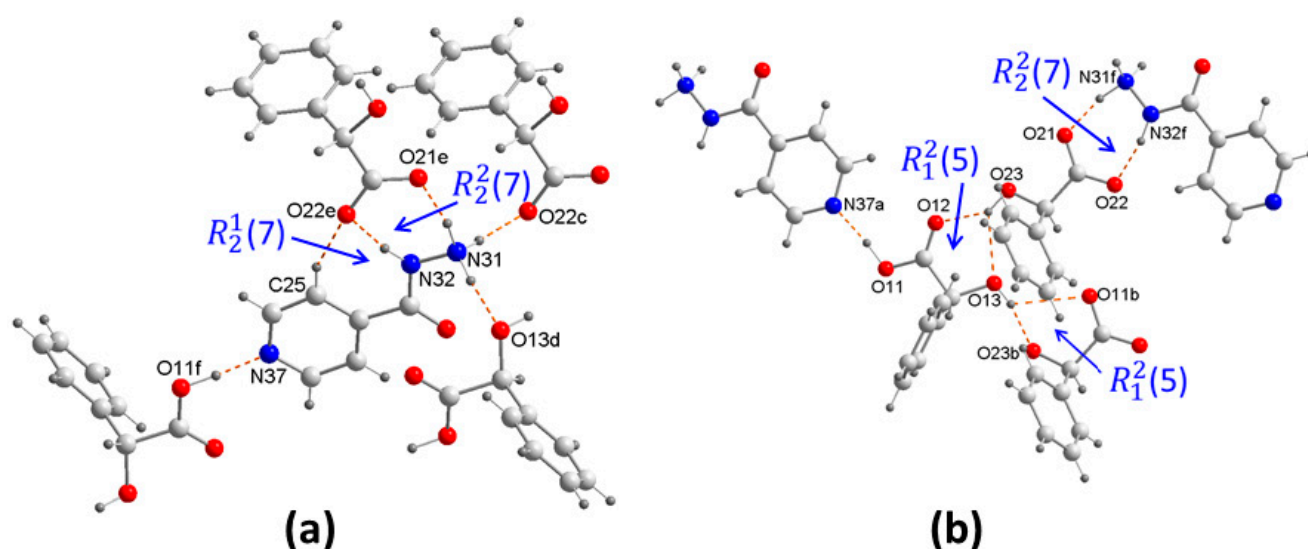
Figure 5. Detail of the packing in **2** showing the interactions between (**a**) Hinh$^+$ and Hma$^-$/H$_2$ma and (**b**) between Hma$^-$/H$_2$ma and Hinh$^+$.
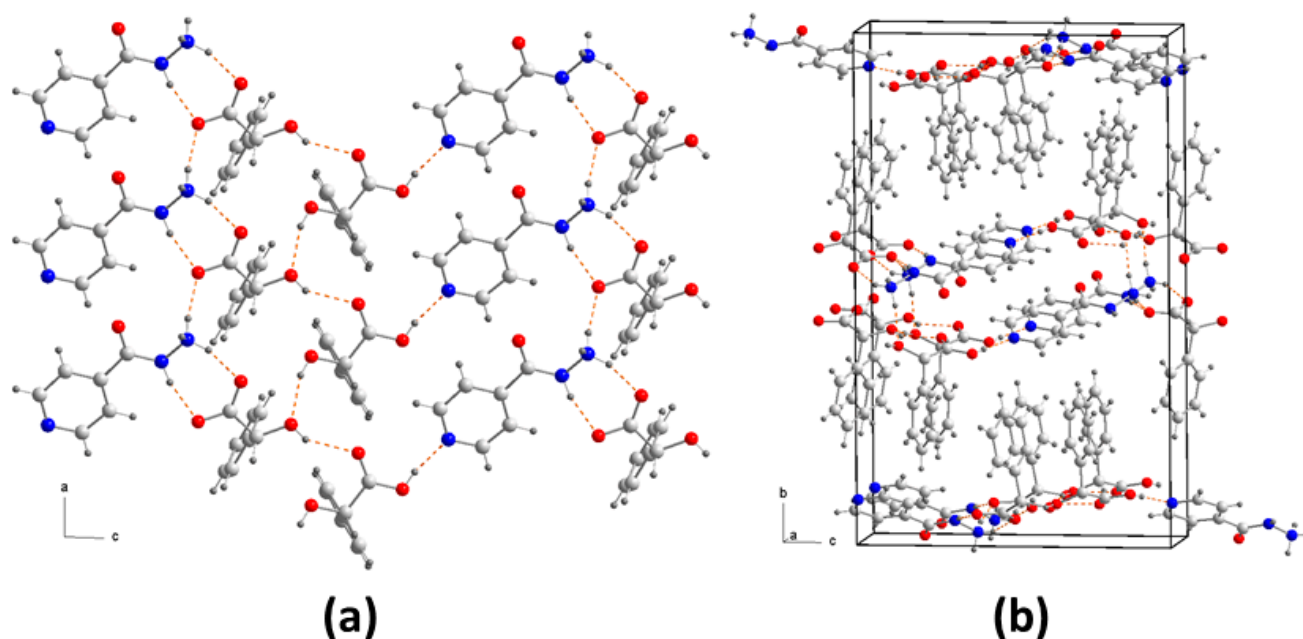

Figure 6. (**a**) View of a layer parallel to the "ca" plane at **2**, and (**b**) perspective of the crystalline package.

Compound 3. N′-(propan-2-ylidene)isonicotin-hydrazide hemihydrate, (**3**), was prepared by adapting the crystallization method described in the literature [52]. The product was obtained by the co-crystallization of isoniazid and glycolic acid from acetone at room temperature. Slow evaporation of the solvent under ambient conditions produced single crystals of (**3**). The process consists of a one-pot synthesis, with covalent modification occurring in situ, where inh is reacted with acetone, or in general with molecules containing ketone or aldehyde functional groups (RC=O), so that the NH$_2$ group of the carbohydrazide moiety undergoes a condensation reaction and replaces the two H atoms with alkyl groups to form isonicotin-hydrazides (Scheme 2). This technique is similar to what has been called "covalence-assisted supramolecular synthesis", with the difference that in this case a hemihydrate has been obtained instead of a cocrystal with a glycolic acid molecule as co-former, as expected [53]. The asymmetric unit of **3** contains one N′-(propan-2-ylidene)isonicotin-hydrazide molecule and half a molecule of water. Figure 7 shows the crystal structure of pinh.
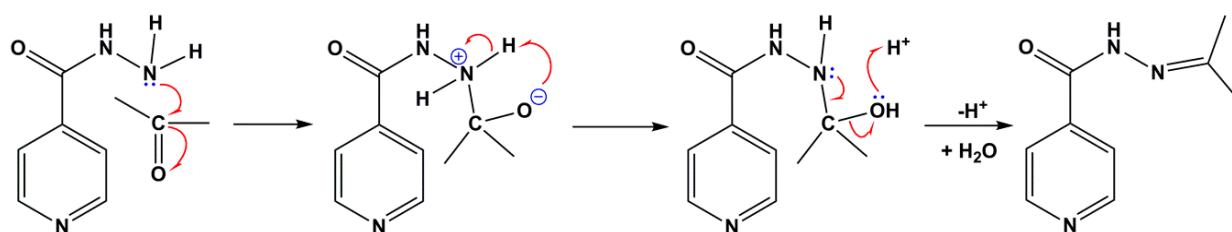
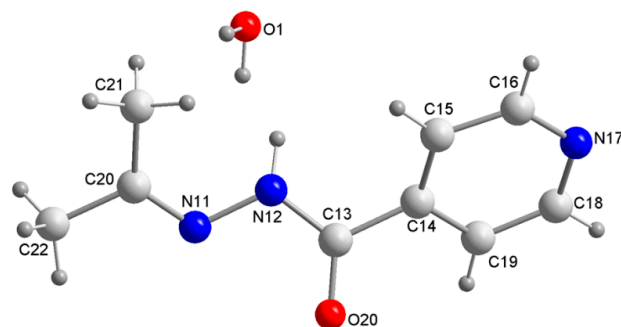**Scheme 2.** Mechanism for the formation of N′-(propan-2-ylidene)isonicotin hydrazide from isoniazid.

Figure 7. Asymmetric unit of (pinh)·1/2(H$_2$O) (**3**) showing the atom-numbering scheme.

The distances and angles within the pinh are as expected. The crystal structure of **3** shows a substantial change in the pattern and packing of hydrogen bonds with respect to the structures of **1** and **2**. The replacement of the two hydrazine hydrogen atoms by the isopropylidene group set aside most of the functionality of the hydrogen bonds of isoniazid. Likewise, the presence of half a molecule of water in the crystalline structure instead of a COOH group of a carboxylic acid, when this is a co-former in a cocrystal with the modified isoniazid, gives rise to a different packing. The crystal structure consists of a 1D network of *C*(4) chains formed by homomeric hydrogen bonding of the amide group, i.e., N12−H12A···O20, linking symmetrically related pinh molecules to form chains along the c-axis (Figure 8a).
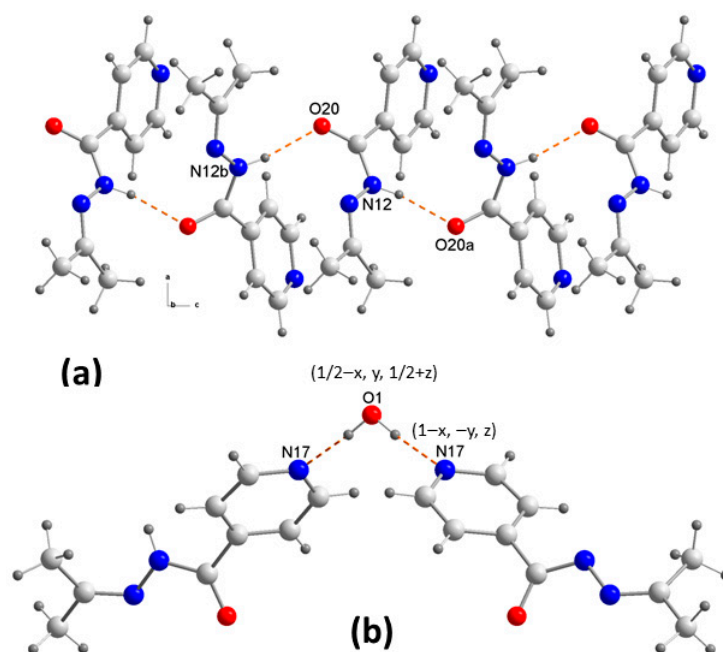

Figure 8. Detail of the crystal packing at **3** showing (**a**) the formation of pinh chains along the c axis and (**b**) a water molecule bridging between two pinh molecules.

Such chains have been observed in N'-(propan-2-ylidene)isonicotino-hydrazide cocrystals with carboxylic acids [52,53]. Furthermore, the characteristic carboxylic acid-pyridine hetero-synton of $R_2^2(7)$ graph-set motif [52,53], that is formed between the COOH group and the N'-(propan-2-ylidene)isonicotin-hydrazide molecule in carboxylic acid cocrystals with the modified isoniazid, in (**3**) is replaced by a water-pyridine hydrogen bond (Figure 8b). Thus, each water molecule acts as a bridge joining two chains of pinh molecules (Figure 9a) to form a 2D structure extending in a zigzag parallel to the "ac" (Figure 9a).
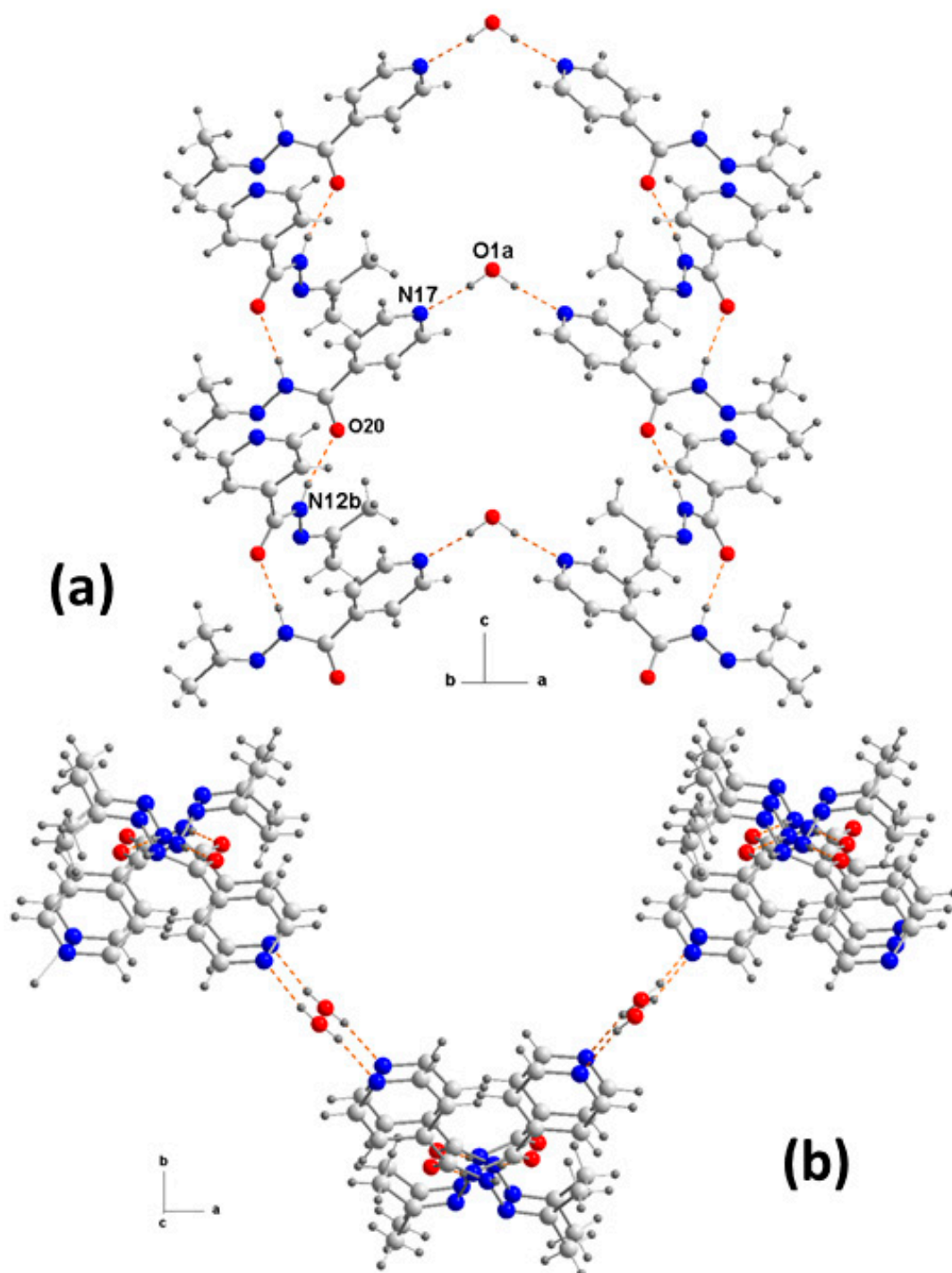

Figure 9. Detail of the crystalline packing in **3** projected (**a**) on the ac plane and (**b**) on the ab plane.

The crystal packing is reinforcing by the existence of some non-classical hydrogen bonds (Table 2), where a C–H bond of a methyl group (C22) and another of the pyridine ring (C19) act as donors against the oxygen atom of the molecule of water, which acts as an acceptor, and a second C–H bond of the pyridine ring (C16) against the oxygen atom of the organic molecule, as an acceptor (Figure 10).
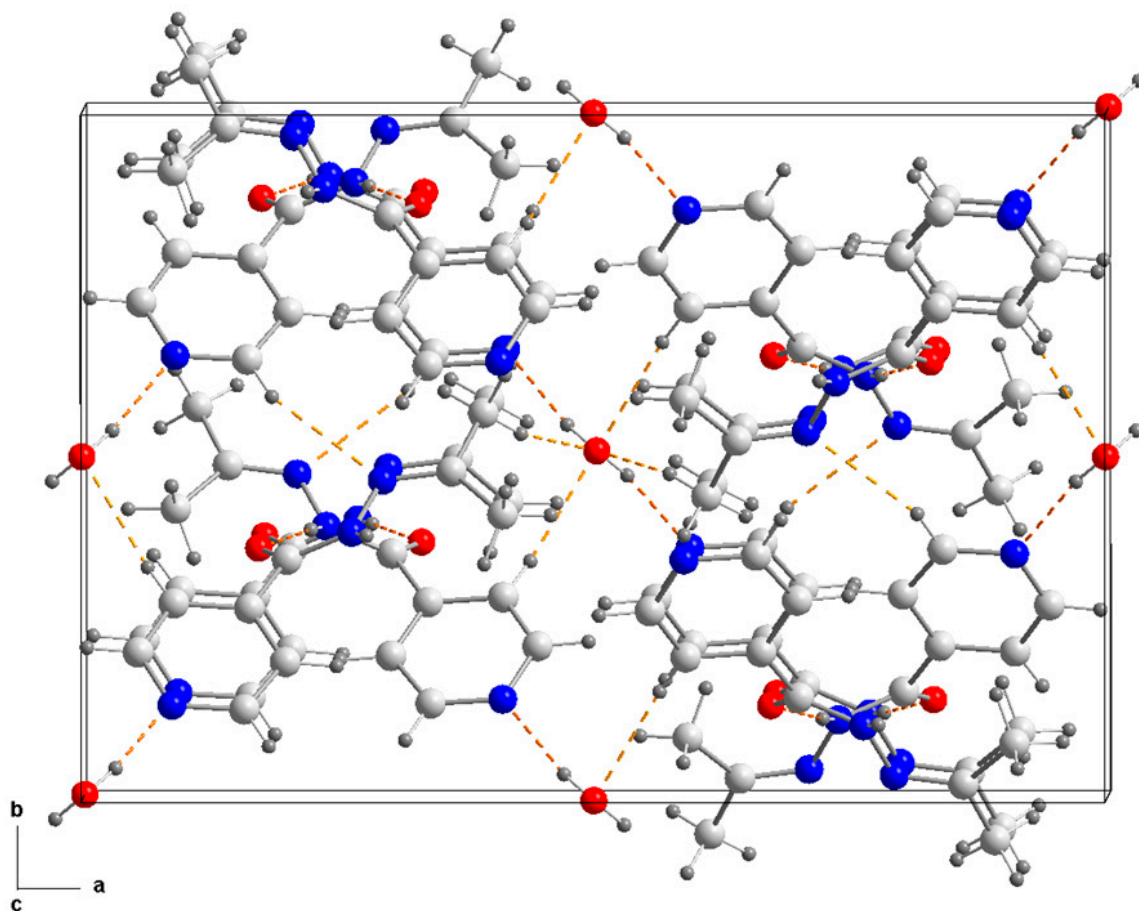

Figure 10. Projection on the ab plane of the unit cell of **3**.

3.2. Hirshfeld Surface Analysis

To explore and quantify the intermolecular interactions that are responsible for the crystal packing of compounds **1**–**3**, the Hirshfeld surfaces (hs) and two-dimensional fingerprint (FP) plots were plotted. A view of the Hirshfeld surfaces mapped over d_{norm} function is shown in Figure 11, highlighting the main inter-molecular contacts. In addition, the HS mapped over the shape index and curvedness properties for compounds **1** and **2** are shown in Figure 12. The full fingerprint plots for **1**–**3** are displayed in Figure 13.
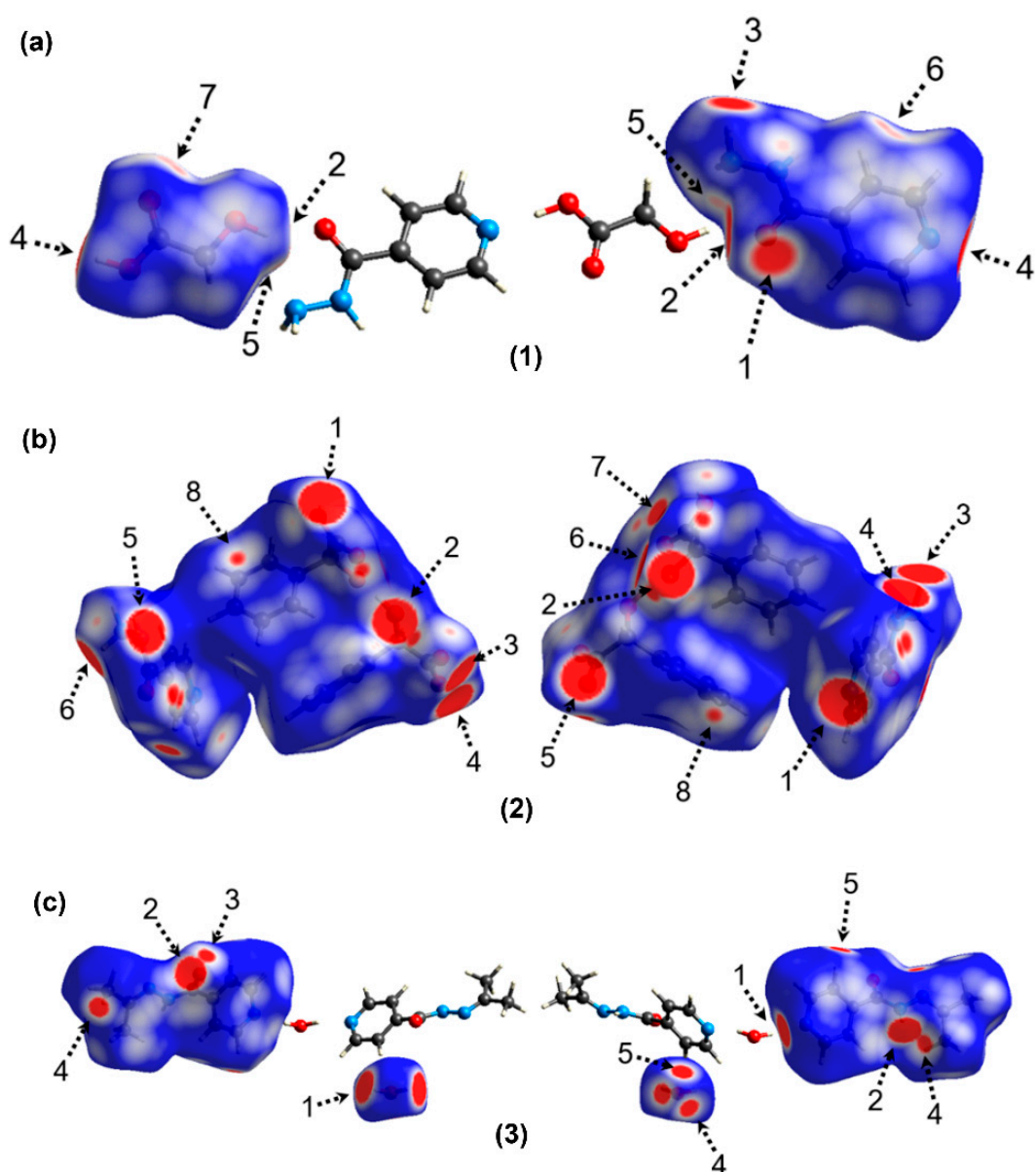
Figure 11. View of the Hirshfeld surfaces of compounds **1–3** mapped with d$_{norm}$ function. In **2**, the Hirshfeld surface is shown in two orientations, front and back view. The labels are discussed in the main text.
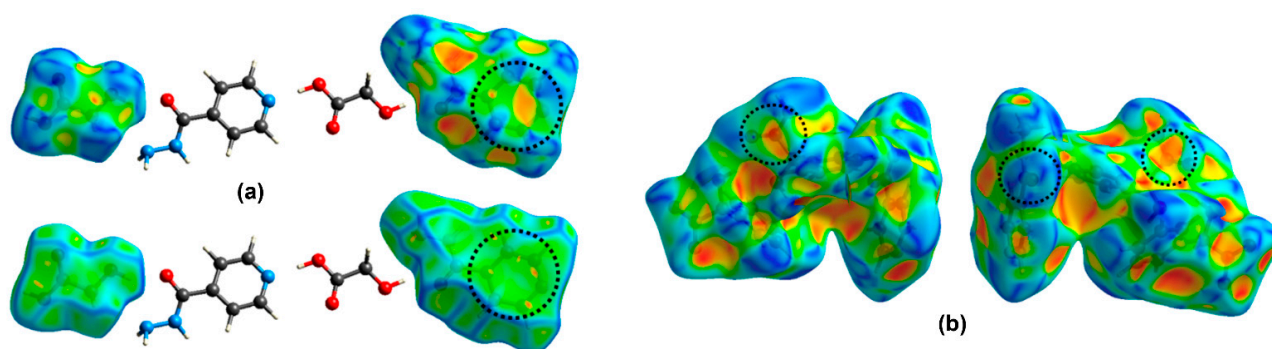

Figure 12. (**a**) View of the Hirshfeld surfaces mapped over shape index (top) and curvedness (button) property of compound **1**; (**b**) Hirshfeld surfaces mapped over shape index property of **2** showing the C=O···C=O interactions. The regions involved in the π···π and C=O···C=O interactions are highlighted by black dashed circles.
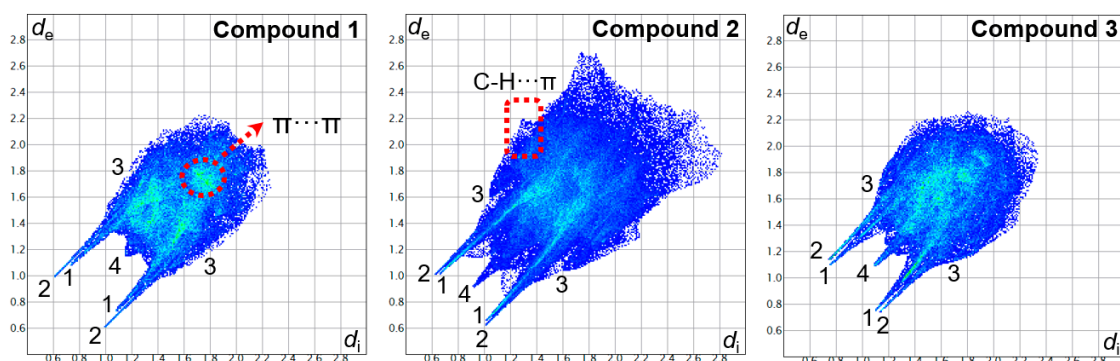
Figure 13. The full two-dimensional fingerprint plots of compounds **1**–**3** showing: (1) H···O/O···H, (2) H···N/N···H, (3) H···C/C···H and (4) H···H contacts.

H···H contacts represent the largest contribution (33.4%, 37.4% and 47.8% for 1, 2 and 3, respectively), and they are highlighted in the middle of scattered points in the FP plots (Figure 3) with a minimum value of ($d_e + d_i \approx 2.0$ Å), shorter than the sum of vdW radii.

In compound 1, the bright-red spot labeled 1 on the HS shows H···O/O···H contacts associated with N11–H11A···O20 hydrogen bonds. The bright-red regions labeled as 2 are associated with O13–H13A···O20 hydrogen bonds, which constitute the strongest among all interactions present in 1. The large red region labeled 4 is attributed to O11–H11···N17 which are mainly responsible for the strong interaction between isoniazide and glycolic acid. The red spot labeled 7 is assigned to N12–H12A···O12 hydrogen bonding interactions involving the N–H group of isoniazide and the O12 atom of glycolic acid as acceptor. Additionally, the small red spot labeled 6 is attributed to C15–H15···O12 hydrogen bonds. These H···O/O···H contacts are also identified by a pair of symmetrical sharp spikes at ($de + di \approx 1.8$ Å) in the FP plot (Figure 13) with 37.5 % contribution to the total HS area. The H···N/N···H contacts labeled 3 and 5 appear as red spots in the d_{norm} surface attributed to N11–H11B···N12 and O13–H13A···N11 hydrogen bonds, respectively. These interactions are also visible in the FP plot as two sharp spikes at ($de + di \approx 1.6$ Å), with a contribution of 11.3 % to the total HS area. The broad spikes labeled 3 in the FP plot are indicative of H···C/C···H contacts with a contribution of 8.0 % of the total HS area.

In addition to these hydrogen bonds, the supramolecular assembly of compound **1** is also stabilized by $\pi \cdots \pi$ stacking interactions involving the pyridine ring of isoniazide. These interactions show an inter-centroid distance of 3.893 Å. These contacts are visible in the HS mapped over shape index and curvedness properties (Figure 12).

The complementary pair of red and blue triangles (highlighted as dashed lines) in shape index and the green flat area in curvedness are characteristic of $\pi \cdots \pi$ stacking interactions. In addition, the FP plot shows a green area around $d_e = d_i = 1.8$ Å that corresponds to $\pi \cdots \pi$ stacking interactions (6.60 % of total contribution).

In compound **2**, the large bright area labeled 1 in the d_{norm} surface (Figure 11) represents H···N/N···H contacts which are attributed to O11–H11···N37 hydrogen bonds involving the pyridinic N37 atom of isoniazide and the H11 atom of the mandelic acid. These interactions are represented as a pair of symmetrical spikes at ($d_e + d_i \approx 1.6$ Å) in FP, and comprise 4.90 % of the total Hirshfeld surface area. The bright-red spots labeled 2 to 6 are attributed to O13–H13···O23, N31–H31C···O21, N32–H32···O22, N31–H31A···O22 and N31–H31B···O13 hydrogen bonds, respectively. The proportion of H···O/O···H contacts comprises 31.4 % of the total HS area. The presence of H···C/C···H contacts (19.8 %) is identified by both diminutive spots and red regions labeled 8. One of these spots is located in the phenyl (C13–C18) ring and the second is located at around the H27 atom from a neighboring molecule (H···Cg distance = 2.818 Å). These features support the relevance of C–H···π interactions in the supramolecular assembly of **2**. These C–H···π contacts appear in a characteristic form of pronounced 'wings' on both sides of FP. The crystal packing of **2** is also stabilized by C=O···C=O interactions involving the O40 atom of isoniazide and the

C11=O12 group of mandelic acid [d(O40···C11) = 2.931 Å]. The existence of C=O···C=O interactions can be seen on the HS mapped over shape index property (Figure 2b), showing surface patches with a large red depression above the C11=O12 carbonyl group, and a blue region surrounding the O40 atom. The C···O/O···C contacts show a notable contribution of 4.50% to the HS area.

The d_{norm} surface of compound **3** highlights the short intermolecular interactions which are responsible for the crystal stabilization of the co-crystal formed by isoniazide and water. The H···N/N···H contacts labeled 1 in the d_{norm} mal of **3** (Figure 11) are dominant, appearing as large deep-red spots attributed to O1–H1A···N17 hydrogen bonds. These interactions are also observed as two sharp spikes in FP with short ($d_e + d_i \approx 1.9$ Å) and a contribution of 16.9 % to the total HS area. The large red spots labeled 2 are attributed to N12–H12A···O20 involving the N–H and the carbonyl groups of isoniazide. The small red spots labeled 3 and 4 are assigned to C21–H21B···O20 and C22–H22C···O1 hydrogen bonds, respectively. In addition, the light red spots labeled 5 in the d_{norm} map are due to C19–H19···O1 involving the H19 atom of the isoniazide and the O1 atom of water molecule. The proportion of H···O/O···H contacts comprises 18.1 % of the total HS area.

3.3. DFT Calculations

3.3.1. Compound **1**

First, we have computed the molecular electrostatic potential surface of the two co-formers of cocrystal **1** and represented them in Figure 14. The maximum molecular electrostatic potential surface (MEP) value in glycolic acid is located, as expected, at the carboxylic H-atom (+55 kcal/mol) and the minimum in the middle of the O-atoms of carboxy and hydroxy groups (−49 kcal/mol). The value at the hydroxy H-atom is also large and positive (+47 kcal/mol). The maximum and minimum MEP values in isoniazide are located at the amido group (+44 kcal/mol and −42 kcal/mol, respectively). The MEP is also significant at the pyridinic N-atom is (−25 kcal/mol) and the NH_2 group (+31 kcal/mol) of isoniazid. Overall, the MEP surface analysis confirms the strong ability of both compounds to participate in H-bonding interactions both as donor and acceptors.
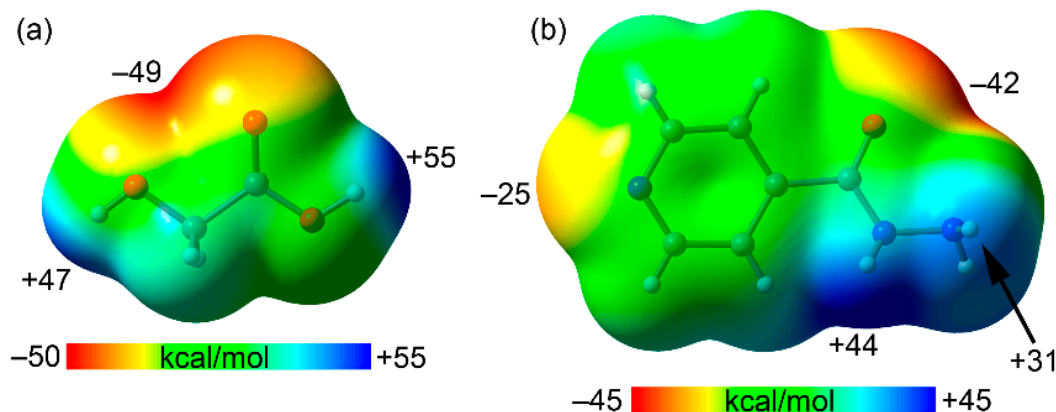

Figure 14. MEP surfaces of Glycolic acid (**a**) and isoniazid (**b**) at the PBE0-D3/def2-TZVP. Iso-surface 0.001 a.u. The MEP values at selected points of the surfaces are given in kcal/mol.

The cocrystal **1** forms infinite 1D chains in the solid state where the H_2ga connects two isoniazid molecules by means of H-bonding interactions. We have used a trimer extracted from this infinite chain to analyze the H-bonding interactions energetically and, using the quantum theory of atoms in molecules (QTAIM) and non-covalent interactions (NCIplot) index analyses, the results are gathered in Figure 15.
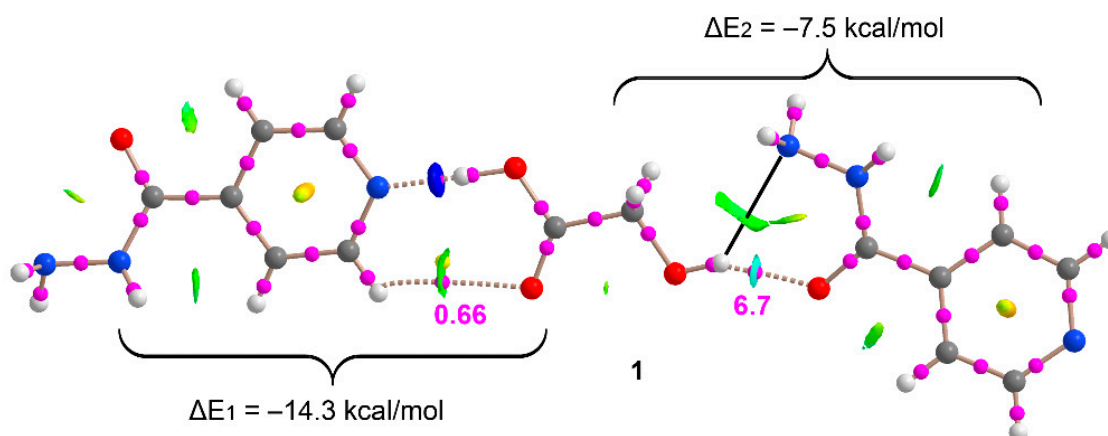
Figure 15. Distribution of bond and ring critical points (CPs) (magenta and yellow spheres, respectively) and bond paths in a trimeric assembly of **1**. The dissociation energies of the H-bonds are indicated adjacent to the bond CPs. NCIPlot index analysis is also shown. RDG iso-surface 0.5 a.u., density cutoff = 0.06 a.u., Color range: -0.05 a.u. $\leq$ sign($\lambda2$)$\rho \leq 0.05$ a.u.

The carboxylic acid of H_2ga interacts with the pyridine ring forming two H-bonds as revealed by the QTAIM analysis. A bond CP (magenta sphere) and bond path connect the H-atom of the COOH group to the N-atom of pyridine. Moreover, an ancillary C–H···O contact is also established and characterized by the corresponding bond CP and bond path. The NCIplot index confirms the existence of both interactions and reveals that the O–H···N is very strong (dark blue iso-surface) and the C–H···O is weak (green and small iso-surface). The formation energy of this dimer is large and negative ($\Delta E_1 = -14.3$ kcal/mol) thus confirming the strong nature of the O–H···N H-bond. In fact, we have estimated the H-bond dissociation energy of the C–H···O using the potential energy density at the bond CP using the formula proposed by Espinosa et al. [37] ($E_{dis} = -0.5V_r$). Several investigations have demonstrated the utility of QTAIM derived from experimental data to evaluate H-bonding and π-stacking interactions [54–56]. The dissociation energies are represented in magenta in Figure 15. It can be observed that the energy of the C–H···O contact is only 0.66 kcal/mol, and consequently the O–H···N energy is approximately -13.64 kcal/mol, confirming its strong nature, in agreement with the short experimental distance. The H_2ga is also connected to another isoniazid molecule (thus propagating the 1D supramolecular polymer) by a O–H···O bond that is characterized by the corresponding bond CP and bond path. This H-bond is moderately strong (6.7 kcal/mol), see Figure 15. The NCIplot analysis shows that there is also an attractive interaction between the N-atom of the NH_2 group and the H-atom, via the available lone pair, since a green iso-surface is located between both atoms. The difference between the dimerization energy ($\Delta E_2 = -7.5$ kcal/mol) and the dissociation energy of the O–H···O bond (6.7 kcal/mol) is a rough estimation of the H_2N···H–O interaction, which is -0.8 kcal/mol. The large interaction energies of both OH···N,O H-bonds at both ends of the H_2ga explains the formation of the 1D supramolecular chain in **1**.

3.3.2. Compound **2**

For compound **2**, where cationic and anionic forms of isoniazid and mandelic acid, respectively, are present in the solid state structure, we have limited the study to the evaluation of the H-bonds using the QTAIM analysis, since it is convenient to estimate the H-bonding energies without the large contribution of the pure coulombic attraction between the counter-ions. The QTAIM analysis of a trimeric assembly of **2** is shown in Figure 16 and it can be observed that the H-bonds established between the counterions (charge assisted HBs) are very strong and characterized by the corresponding bond CPs, bond paths and dark blue NCIPlot index iso-surfaces. The H-bonds established between the neutral and anionic mandelic acids are significantly weaker, as revealed by both the color of the NCIplot and the dissociation energies. In the latter a bifurcated H-bond is

observed, where the hydroxyl group of the mandelate is connected via two bond CPs and bond paths to the O-atoms of the hydroxyl and carboxy groups of the neutral mandelic acid.
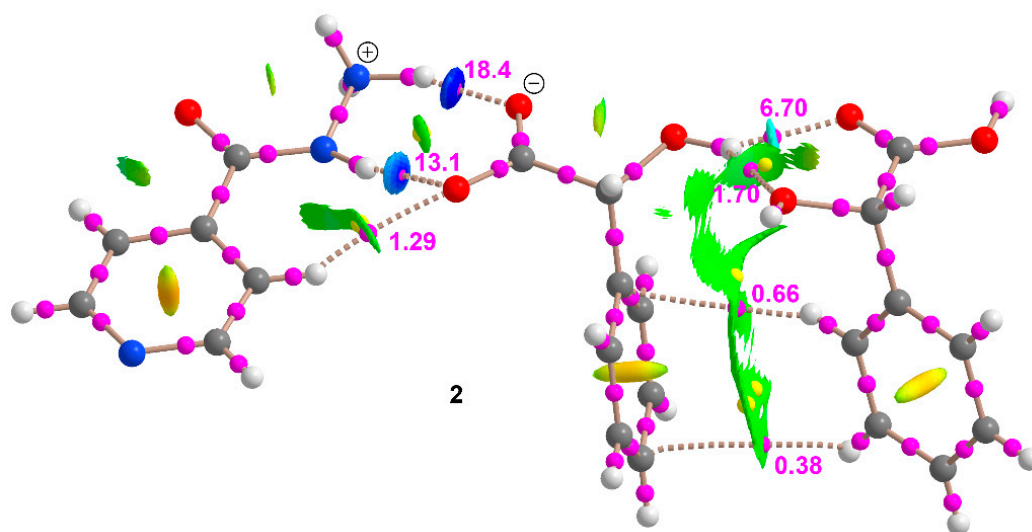

Figure 16. Distribution of bond and ring critical points (pink and yellow spheres, respectively) and bond paths in a trimeric assembly of **2**. The dissociation energies of the H-bonds are indicated adjacent to the bond CPs. NCIPlot index analysis is also shown. RDG iso-surface 0.5 a.u., density cutoff = 0.06 a.u., Color range: –0.05 a.u. $\leq$ sign(λ_2)ρ $\leq$ 0.05 a.u.

3.3.3. Compound **3**

The MEP surface of compound **3** is represented in Figure 17, revealing that the maximum and minimum MEP values are located at the amido group, as expected. The minimum is displaced toward the N-atom of the imino group due to the influence of the lone pair on the sp^2 hybridized N-atom. The MEP value at the pyridinic N-atom is also large and negative (-35 kcal/mol).
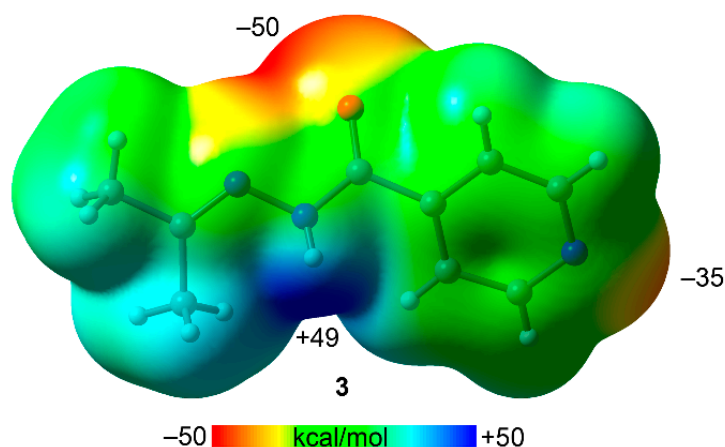

Figure 17. MEP surface of compound **3** at the PBE0-D3/def2-TZVP. Iso-surface 0.001 a.u. The MEP values at selected points of the surface are given in kcal/mol.

The QTAIM/NCIPlot index analysis of the H-bonded dimer observed in the solid state of compound **3** is given in Figure 18. The dimerization energy is large and negative ($\Delta E_3 = -16.6$ kcal/mol) confirming that it is an important synthon. The NH group that forms the H-bond is displaced toward the N-atom of the imino group in good agreement with the MEP surface analysis. The QTAIM distribution of critical points and bond paths reveals the existence of two additional CO$\cdots$H–C contacts involving both aliphatic and aromatic C–H groups. The sum of the H-bond energies is 7.27 kcal/mol using the V_r

predictor (values in magenta in Figure 18). The comparison of the H-bonds with the dimerization energy suggests that the π-interaction between the pyridine ring and the dimethyl-imino group is very relevant. In fact, the NCIplot shows a large green iso-surface located between the pyridine and the $Me_2C=N$ moiety, confirming the existence of the van der Waals interaction. Moreover, the QTAIM analysis shows the existence of two bond CPs and both paths that connect two aromatic C-atoms to the imino N-atom and one H-atom of the methyl group.
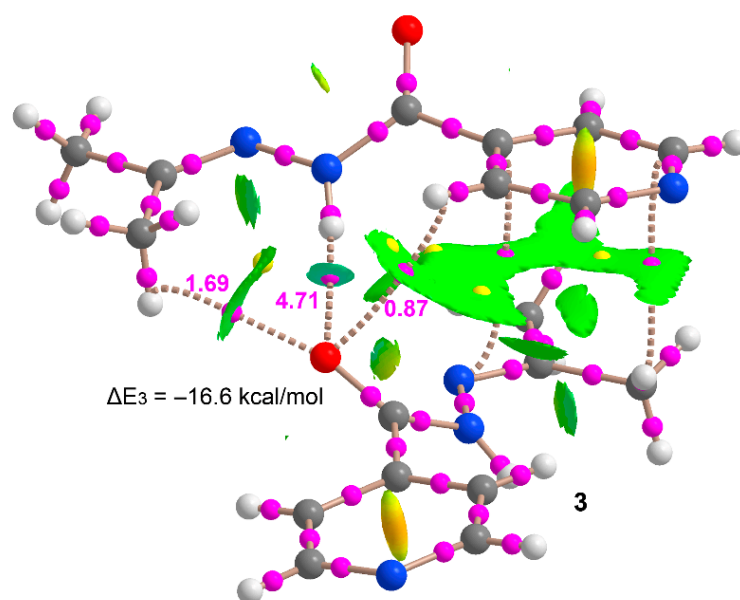

Figure 18. Distribution of bond and ring critical points (magenta and yellow spheres, respectively) and bond paths in a dimer of **3**. The dissociation energies of the H-bonds are indicated adjacent to the bond CPs. NCIPlot index analysis is also shown. RDG iso-surface 0.5 a.u., density cutoff = 0.06 a.u., Color range: -0.05 a.u. $\leq sign(\lambda_2)\rho \leq 0.05$ a.u.

3.3.4. Comparison of H-Bond Energies in Compounds 1–3 with Experimental Values from the Literature

The energy of the C–H⋯O H-bonds described above for compounds **1–3** range from 0.66 to 1.69 kcal/mol, those of the neutral OH⋯O and NH⋯O H-bonds range from 6.7 to 13.1 and the charge assisted H-bond in **2** is 18.4 kcal/mol. These values agree quite well with the experimental energies reported by Borissova et al. [57] for adducts of collidine with benzoic acids. In this study, the experimental energy reported for the C–H⋯O interaction was 0.7 kcal/mol and those for the charge assisted N^+–H⋯O^- H-bonds between collidinium and several benzoate acids were of the order of 22.9 kcal/mol.

4. Concluding Remarks

Co-crystallization involving isoniazid (inh) and glycolic acid (H_2ga) or mandelic acid (H_2ma), leads to the formation of a cocrystal of composition (inh) (H_2ga) (**1**) and a salt-cocrystal containing the isoniazide-ammonium cation, monoanion mandelate and a molecule of mandelic acid (**2**). In addition, a semi-hydrate of N′-(propan-2-ylidene)isonicotin-hydrazide (**3**) has been obtained in a condensation of inh with a propanone molecule in the presence of H_2ga. These cocrystals have been designed to explore the diversity of supramolecular synthons between inh and α-hydroxycarboxylic acids. Analysis of the molecular structure and crystalline packing reveals that the typical carboxylic acid–pyridine and hydroxyl-carbonyl hetero-synthons are present in **1**. In **2**, in addition to the acid-pyridine synthon, there are also, among others, carboxylate-hydrazonium hetero-synthons. In **3**, water-pyridine synthons replace the typical carboxylic acid-pyridine and a hetero-synthon hydrazine-carboxylate is responsible for their crystalline packing. From

the FT-IR spectra, it was possible to confirm the formation of the co-crystal and the salt, as well as the absence of glycolic acid in compound **3**. The non-covalent interactions were evaluated using the Hirshfeld surface analysis and DFT calculations. The hydrogen bonds are dominant forces in the stabilization of the cocrystals. Their individual contributions have been estimated using the potential energy density at the bond CPs and in some cases they are very strong (up to 18.4 kcal/mol). In compound **3**, the π-stacking of pyridine and the dimethyl-imino group is also energetically relevant.

Supplementary Materials: The following are available online at https://www.mdpi.com/2073-435 2/11/4/328/s1, FT-IR and NMR spectra of all compounds.

Author Contributions: Conceptualization, R.Á.-V., I.G.-S., R.T.-I. and J.M.G.-P.; methodology, R.Á.-V., I.G.-S., R.T.-I. and J.M.G.-P.; software, A.F. and D.M.G.; validation, A.C., A.F., J.N.-G. and D.M.G.; formal analysis, R.Á.-V., I.G.-S., R.T.-I. and J.M.G.-P.; investigation, R.Á.-V., I.G.-S., R.T.-I., J.M.G.-P. and D.M.G.;Data curation, R.Á.-V., I.G.-S. and R.T.-I.; writing—original draft preparation, A.C.; writing—review and editing, A.C., A.F. and D.M.G.; visualization, R.Á.-V., I.G.-S., R.T.-I. and J.M.G.-P.; supervision, A.C., J.N.-G. and A.F.; project administration, A.C. and A.F.; funding acquisition, A.C. and A.F. All authors have read and agreed to the published version of the manuscript.

Institutional Review Board Statement: Not applicable.

Informed Consent Statement: Not applicable.

Data Availability Statement: Not applicable.

Conflicts of Interest: The authors declare no conflict of interest.

References

1. Stahly, G.P. A Survey of Cocrystals Reported Prior to 2000. *Cryst. Growth Des.* **2009**, *9*, 4212–4229. [CrossRef]
2. Du, M.; Zhang, Z.H.; Wang, X.G.; Wu, H.F.; Wang, Q. Flexible Building Blocks of N,N'-Bis(picolinoyl)hydrazine for Hydrogen-Bonding Directed Cocrystallization: Structural Diversity, Concomitant Polymorphs, and Synthon Prediction. *Cryst. Growth Des.* **2006**, *6*, 1867–1875. [CrossRef]
3. Wouters, J.; Quere, L. (Eds.) *Pharmaceutical Salts and Co-Crystals*; RSC Drug Discovery Series No. 16; RSC Publisher: Cambridge, UK, 2011.
4. Diniz, L.F.; Souza, M.S.; Carvalho, P.S., Jr.; da Silva, C.C.P.; D'Vries, R.F.; Ellena, J. Novel Isoniazid cocrystals with aromatic carboxylic acids: Crystal engineering, spectroscopy and thermochemical investigations. *J. Mol. Struct.* **2018**, *1153*, 58–68. [CrossRef]
5. Foces-Foces, C.; Llamas-Saiz, A.L.; Lorente, P.; Golubev, N.S.; Limbach, H.-H. Three 2,4,6-trimethylpyridine-benzoic acid complexes at 150 K. *Acta Cryst.* **1999**, *C55*, 377–381.
6. Seaton, C.C. Proton location in acid⋯pyridine hydrogen bonds of multi-component crystals. *CrystEngComm* **2014**, *16*, 5878–5886. [CrossRef]
7. Oruganti, M.; Khade, P.; Dasc, U.K.; Trivedi, D.R. The hierarchies of hydrogen bonds in salts/cocrystals of isoniazid and its Schiff base—A case study. *RSC Adv.* **2016**, *6*, 15868–15876. [CrossRef]
8. Mironov, A.V.; Tafeenko, V.A.; Grebenkin, D.Y.; Oblezov, A.E. Hydrogen bonding in hydroxypyridium salts. *Z. Kristallogr.* **2018**, *233*, 501–506. [CrossRef]
9. Goswami, P.K.; Kumar, V.; Ramanan, A. Multicomponent solids of diclofenac with pyridine based coformers. *J. Mol. Struct.* **2020**, *1210*, 128066. [CrossRef]
10. Shattock, T.R.; Arora, K.K.; Vishweshwar, P.; Zaworotko, M.J. Hierarchy of Supramolecular Synthons: Persistent Carboxylic Acid⋯Pyridine Hydrogen Bonds in Cocrystals That also Contain a Hydroxyl Moiety. *Cryst. Growth Des.* **2008**, *8*, 4533–4545. [CrossRef]
11. Iseman, M.D. Tuberculosis therapy: Past, present and future. *Eur. Respir. J.* **2002**, *20* (Suppl. 36), 87s–94s. [CrossRef]
12. Hearn, M.J.; Cynamon, M.H.; Chen, M.F.; Coppins, R.; Davis, J.; Kang, H.J.-O.; Noble, A.; Tu-Sekine, B.; Terrot, M.S.; Trombino, D.; et al. Preparation and antitubercular activities in vitro and in vivo of novel Schiff bases of isoniazid. *Eur. J. Med. Chem.* **2009**, *44*, 4169–4178. [CrossRef]

13. Lemmerer, A. Covalent assistance to supramolecular synthesis: Modifying the drug functionality of the antituberculosis API isoniazid in situ during co-crystallization with GRAS and API compounds. *CrystEngComm* **2012**, *14*, 2465–2478. [CrossRef]

14. Sarcevica, I.; Orola, L.; Veidis, M.V.; Podjava, A.; Belyakov, S. Crystal and Molecular Structure and Stability of Isoniazid Cocrystals with Selected Carboxylic Acids. *Cryst. Growth Des.* **2013**, *13*, 1082–1090. [CrossRef]

15. Aitipamula, S.; Wong, A.B.H.; Shan Chowa, P.; Tan, R.B.H. Novel solid forms of the anti-tuberculosis drug, Isoniazid: Ternary and polymorphic cocrystals. *CrystEngComm* **2013**, *15*, 5877–5887. [CrossRef]

16. Castiñeiras, A.; García-Santos, I.; González-Perez, J.M.; Bauzá, A.; Zaręba, J.K.; Niclós-Gutiérrez, J.; Torres, R.; Vilchez, E.; Frontera, A. Multicomponent Supramolecular Assemblies of Melamine and α-hydroxycarboxylic Acids: Understanding the Hydrogen Bonding Patterns and Their Physicochemical Consequences. *Cryst. Growth Des.* **2018**, *18*, 6786–6800. [CrossRef]

17. Alvarez-Lorenzo, C.; Castiñeiras, A.; Frontera, A.; García-Santos, I.; González-Pérez, J.M.; Niclós-Gutiérrez, J.; Rodríguez-González, I.; Vílchez-Rodríguez, E.; Zaręba, J.K. Recurrent motifs in pharmaceutical cocrystals involving Glycolic acid: X-ray characterization, Hirshfeld surface analysis and DFT calculations. *CrystEngComm* **2020**, *22*, 6674–6689. [CrossRef]

18. Zhou, Z.-H.; Hou, S.-Y.; Cao, Z.-X.; Wan, H.-L.; Ng, S.-W. Syntheses, crystal structures and biological relevance of glicolato and S-lactato molybdates. *J. Inorg. Biochem.* **2004**, *98*, 1037–1044. [CrossRef] [PubMed]

19. Tumanova, N.; Payen, R.; Springuel, G.; Norberg, B.; Robeyns, K.; Le Duff, C.; Wouters, J.; Leyssens, T. Cocrystallization out of the blue: Dl-mandelic acid/ethyl-DL-mandelate cocrystal. *J. Mol. Struct.* **2017**, *1127*, 397–402. [CrossRef]

20. Brunner, H.; Maiterth, F.; Treittinger, B. Synthesis and antitumor activity of water-soluble 2-benzyl-1,2-diaminobutane-α-oxycarboxylatoplatinum(II) complexes. *Inorg. Chim. Acta* **1992**, *200*, 79–84. [CrossRef]

21. *Bruker, APEX3 Software*; v2018.7-2; Bruker AXS Inc.: Madison, WI, USA, 2018.

22. Sheldrick, G.M. *SADABS. Program for Empirical Absorption Correction of Area Detector Data*; University of Goettingen: Göttingen, Germany, 1997.

23. Sheldrick, G.M. A short history of SHELX. *Acta Cryst.* **2008**, *A64*, 112–122. [CrossRef] [PubMed]

24. Flack, H.D.; Bernardinelli, G. Absolute structure and absolute configuration. *Acta Cryst.* **1999**, *A55*, 908–915. [CrossRef]

25. Putz, H.; Brandenburg, K. *DIAMOND—Crystal and Molecular Structure Visualization Version 4.6.2*; Crystal Impact GbR: Bonn, Germany, 2020.

26. Spackman, M.A.; Jayatilaka, D. Hirshfeld surface analysis. *CrystEngComm* **2009**, *11*, 19–32. [CrossRef]

27. Spackman, M.A.; McKinnon, J.J. Fingerprinting intermolecular interactions in molecular crystals. *CrystEngComm* **2002**, *66*, 378–392. [CrossRef]

28. McKinnon, J.J.; Jayatilaka, D.; Spackman, M.A. Towards quantitative analysis of intermolecular interactions with Hirshfeld surfaces. *Chem. Commun.* **2007**, *37*, 3814–3816. [CrossRef] [PubMed]

29. Turner, M.J.; McKinnon, J.J.; Wolf, S.K.; Grimwood, D.J.; Spackman, P.R.; Jayatilaka, D.; Spackman, M.A. *CrystalExplorer17*; University of Western Australia: Perth, Australia, 2017.

30. Young, D.; Ding, F.; Lipparini, F.; Egidi, F.; Goings, J.; Peng, B.; Petrone, A.; Henderson, T.; Ranasinghe, D.; Zakrzewski, V.G.; et al. *Gaussian 16, Revision A.01*; Gaussian, Inc.: Wallingford, CT, USA, 2016.

31. Perdew, J.P.; Burke, K.; Ernzerhof, M. Generalized Gradient Approximation Made Simple. *Phys. Rev. Lett.* **1996**, *77*, 3865–3868. [CrossRef] [PubMed]

32. Grimme, S.; Antony, J.; Ehrlich, S.; Krieg, H. A consistent and accurate ab initio parametrization of density functional dispersion correction (DFT-D) for the 94 elements H-Pu. *J. Chem. Phys.* **2010**, *132*, 154104. [CrossRef] [PubMed]

33. Weigend, F.; Ahlrichs, R. Balanced basis sets of split valence, triple zeta valence and quadruple zeta valence quality for H to Rn: Design and assessment of accuracy. *Phys. Chem. Chem. Phys.* **2005**, *7*, 3297–3305. [CrossRef]

34. Bader, R.F.W. A quantum theory of molecular structure and its applications. *Chem. Rev.* **1991**, *91*, 893–928. [CrossRef]

35. *AIMAll*, Version 19.10.12 ed; Todd A. Keith, TK Gristmill Software: Overland Park, KS, USA, 2019; Available online: aim.tkgristmill.com (accessed on 26 February 2021).

36. Boys, S.F.; Bernardi, F. The calculation of small molecular interactions by the differences of separate total energies. Some procedures with reduced errors. *Mol. Phys.* **1970**, *19*, 553–566. [CrossRef]

37. Espinosa, E.; Molins, E.; Lecomte, C. Hydrogen bond strengths revealed by topological analyses of experimentally observed electron densities. *Chem. Phys. Lett.* **1998**, *285*, 170–173. [CrossRef]

38. Efimenko, Z.M.; Eliseeva, A.A.; Ivanov, D.M.; Galmes, B.; Frontera, A.; Bokach, N.A.; Kukushkin, V.Y. Bifurcated μ^2-I⋯(N,O) Halogen Bonding: The Case of (Nitrosoguanidinate)NiII Cocrystals with Iodine(I)-Based σ-Hole Donors. *Cryst. Growth Des.* **2021**, *21*, 588–596. [CrossRef]

39. Zelenkov, L.E.; Ivanov, D.M.; Sadykov, E.K.; Bokach, N.A.; Galmes, B.; Frontera, A.; Kukushkin, V.Y. Semicoordination Bond Breaking and Halogen Bond Making Change the Supramolecular Architecture of Metal-Containing Aggregates. *Cryst. Growth Des.* **2020**, *20*, 6956–6965. [CrossRef]

40. Soldatova, N.S.; Postnikov, P.S.; Suslonov, V.V.; Kissler, T.Y.; Ivanov, D.M.; Yusubov, M.S.; Galmes, B.; Frontera, A.; Kukushkin, V.Y. Diaryliodonium as a double σ-hole donor: The dichotomy of thiocyanate halogen bonding provides divergent solid state arylation by diaryliodonium cations. *Org. Chem. Front.* **2020**, *7*, 2230–2242. [CrossRef]

41. Katlenok, E.A.; Haukka, M.; Levin, O.V.; Frontera, A.; Kukushkin, V.Y. Supramolecular Assembly of Metal Complexes by (Aryl)I⋯dz^2 [PtII] Halogen Bonds. *Chem. Eur. J.* **2020**, *26*, 7692–7701. [CrossRef]

42. Rozhkov, A.V.; Eliseeva, A.A.; Baykov, S.V.; Galmes, B.; Frontera, A.; Kukushkin, V.Y. One-Pot Route to X-perfluoroarenes (X = Br, I) Based on Fe[III]-Assisted C-F Functionalization and Utilization of These Arenes as Building Blocks for Crystal Engineering Involving Halogen Bonding. *Cryst. Growth Des.* **2020**, *20*, 5908–5921. [CrossRef]

43. Rozhkov, A.V.; Ananyev, I.V.; Gomila, R.M.; Frontera, A.; Kukushkin, V.Y. π-Hole$\cdots$dz^2[PtII] Interactions with Electron-Deficient Arenes Enhance the Phosphorescence of PtII-Based Luminophores. *Inorg. Chem.* **2020**, *59*, 9308–9314. [CrossRef]

44. Verdugo-Escamilla, C.; Alarcón-Payer, C.; Frontera, A.; Acebedo-Martínez, F.J.; Domínguez-Martín, A.; Gómez-Morales, J.; Choquesillo-Lazarte, D. Interconvertible Hydrochlorothiazide–Caffeine Multicomponent Pharmaceutical Materials: A Solvent Issue. *Crystals* **2020**, *10*, 1088. [CrossRef]

45. Barbas, R.; Kumar, V.; Vallcorba, O.; Prohens, R.; Frontera, A. Sildenafil–Resorcinol Cocrystal: XRPD Structure and DFT Calculations. *Crystals* **2020**, *10*, 1126. [CrossRef]

46. Johnson, E.R.; Keinan, S.; Mori-Sánchez, P.; Contreras-García, J.; Cohen, A.J.; Yang, W. Revealing Noncovalent Interactions. *J. Am. Chem. Soc.* **2010**, *132*, 6498–6506. [CrossRef]

47. Contreras-García, J.; Johnson, E.R.; Keinan, S.; Chaudret, R.; Piquemal, J.-P.; Beratan, D.N.; Yang, W. NCIPLOT: A Program for Plotting Noncovalent Interaction Regions. *J. Chem. Theor. Comput.* **2011**, *7*, 625–632. [CrossRef]

48. Atta, N.F.; Galal, A.; Ahmed, R.A. Voltammetric Behavior and Determination of Isoniazid Using PEDOT Electrode in Presence of Surface Active Agents. *Int. J. Electrochem. Sci.* **2011**, *6*, 5097–5113.

49. Banerjee, S.S.; Bhanja, K.; Chattopadhyay, P.K. Quantum chemical predictions of aqueous pKa values for OH groups of some α-hydroxycarboxylic acids based on ab initio and DFT calculations. *Comput. Theor. Chem.* **2018**, *1125*, 29–38. [CrossRef]

50. Childs, S.L.; Stahly, G.P.; Pak, A. The Salt−Cocrystal Continuum: The Influence of Crystal Structure on Ionization State. *Mol. Pharm.* **2007**, *4*, 323–338. [CrossRef]

51. Cruz-Cabeza, A.J. Acid–base crystalline complexes and the pK_a rule. *CrystEngComm* **2012**, *14*, 6362–6365. [CrossRef]

52. Lemmerer, A.; Bernstein, J.; Kahlenberg, V. One-pot covalent and supramolecular synthesis of pharmaceutical co-crystals using the API isoniazid: A potential supramolecular reagent. *CrystEngComm* **2010**, *12*, 2856–2864. [CrossRef]

53. Madeley, L.G.; Levendis, D.C.; Lemmerer, A. Covalent-assisted supramolecular synthesis: The effect of hydrogen bonding in cocrystals of 4-tertbutylbenzoic acid with isoniazid and its derivatized forms. *Acta Cryst.* **2019**, *C75*, 200–207. [CrossRef]

54. Kataeva, O.; Nohr, M.; Ivshin, K.; Hampel, S.; Büchner, B.; Knupfer, M. Understanding Intermolecular Interactions in a Tetracene–F4TCNQ Cocrystal via Its Electron Density Distribution and Topology. *Cryst. Growth Des.* **2021**, *21*, 471–481. [CrossRef]

55. Koritsanszky, T.S.; Coppens, P. Chemical Applications of X-ray Charge-Density Analysis. *Chem. Rev.* **2001**, *101*, 1583–1627. [CrossRef]

56. Münch, A.; Knauer, L.; Ott, H.; Sindlinger, C.; Herbst-Irmer, R.; Strohmann, C.; Stalke, D. Insight into the Bonding and Aggregation of Alkyllithiums by Experimental Charge Density Studies and Energy Decomposition Analyses. *J. Am. Chem. Soc.* **2020**, *142*, 15897–15906. [CrossRef]

57. Borissova, A.O.; Lyssenko, K.A.; Gurinov, A.A.; Shenderovich, I.G. Energy Analysis of Competing Non-Covalent Interaction in 1:1 and 1:2 Adducts of Collidine with Benzoic Acids by Means of X-Ray Diffraction. *Z. Phys. Chem.* **2013**, *227*, 775–790. [CrossRef]